On the wind stress and air-ice interactions over the Barents Sea

Dipolmarbeit

von

Katja Weigel

Mathematisch - Naturwissenschaftliche Fakultät der
Christian-Albrechts-Universität zu Kiel
Leibniz - Institut für Meereswissenschaften
Forschungsbereich 1
- Maritime Meteorologie -
and
University Courses in Svalbard

June 7, 2005

Abstract

The connections between the winter wind stress field and the ice conditions in the Barents Sea are examined on interannual time scales between 1970 and 2004. A hindcast data set of wind stress from the Norwegian Meteorological Institute (DNMI) and several ice indices are used. Special attention is given to Storfjorden, a fjord located in the east of the Svalbard, which contains frequently a latent heat polynya. Therefore it is an important source of brine-enriched shelf water.

The ice extent in the Barents Sea turns out to be governed mainly by the meridional wind stress component and to some extent also by the wind stress curl and divergence. Especially in the western and central Barents Sea the wind stress field is influenced by the North Atlantic Oscillation (NAO), while in the easten Barents Sea local processes might be more important.

In Storfjorden a polynya model is used to model the polynya width and total ice production for the winters 2002/2003 and 2003/2004. The polynya width is adjusted to the width estimated from satellite images with factors which are controlling the ability of the polynya to open and close.

An attampt is done to explain the interannual variations of these factors with the help of the wind stress field and ice extent in the areas surrounding Storfjorden.

Zusammenfassung

Untersucht wird der Zusammenhang zwischen dem Windschubfeld und den Eisbedingungen in der Barentssee der Winter 1970 bis 2004. Dazu werden Windschub Hindcast-Daten des Norwegischen Meteorologischen Instituts (DNMI) sowie verschiedene Eisindices genutzt. Das Hauptaugenmerk liegt dabei auf Storfjorden, einem Fjord im Osten Svalbards. Dieser enthält häufig eine Polynya, welche durch nördliche Winde offengehalten wird. Deshalb ist Storfjorden eine wichtige Region für die Produktion von salzreichem Shelfwasser.

Die Eisausdehnung in der Barentssee wird zu einem großen Teil vom meridionalen Windschub bestimmt, wichtig sind aber auch seine Rotation und Divergenz. Besonders im westlichen und zentralen Teil wird das Windstressfeld über der Barentssee von der Nordatlantischen Oszillation (NAO) bestimmt, im östlichen Teil scheinen aber lokale Prozesse wichtiger zu sein.

In Storfjorden wird die Polynyaausdehnung und die Gesamteisproduktion mit Hilfe eines Polynyamodells für die Winter 2002/2003 und 2003/2004 ermittelt. Die Ausdehnung wird mit Faktoren die das Öffnen und Schließen der Polynya kontrollieren an die aus Satellitenbildern ermittelte Ausdehnung angepasst.

Es wird der Versuch unternommen, die jährlichen Schwankungen dieser Faktoren mit Hilfe des Windschubfeldes und der Eisbedingungen im Gebiet um Storfjorden zu erklären.

Contents

1 Introduction

The Barents Sea is one of the shelf seas surrounding the Arctic Ocean, where the variablility of sea ice extent is large, both seasonal and interanual (Vinje and Kvambekk, 1991). It is located between the north coast of the Scandinavian peninsula, the Russian coast between Murmansk and Novaya Zemlya in the south, Franz Josef Land in the northeast and Svalbard in the northwest (Figure 1).

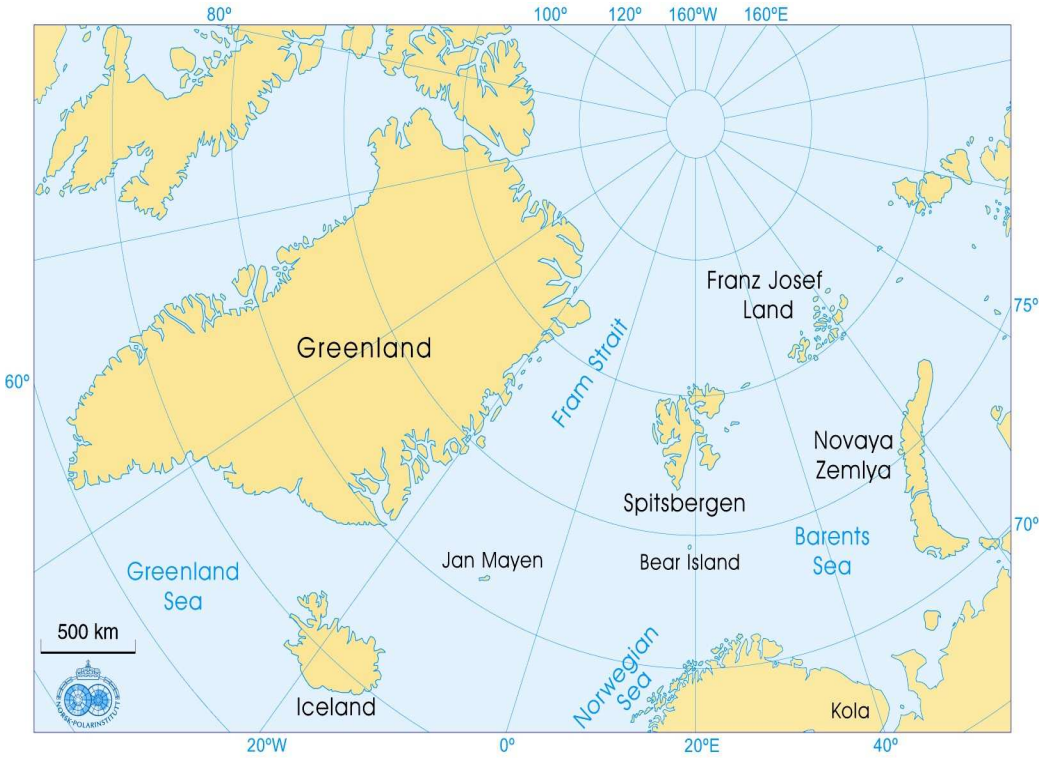

Figure 1: The North Polar region with the Barents Sea, map from Norsk Polarinstitutt (NP) (http://miljo.npolar.no/temakart/pages/homeN.asp).

The sea ice drift is known to be to a large extent influenced by the wind. This was already noticed by Nansen (1902) who found that sea ice drifts in an angle of about 30^o to the right of surface wind.

Sea ice conditions in the Barents Sea became important for whaling and fishing boats, when they started to go to the north. Therefore the first ice observations in the Barents Sea are already known from the 16th century (Loeng 1979). Since these observations were not done routinely and covered only small areas they cannot provide a complete picture of the ice conditions during that time. Routine observations of the ice extent in the whole Barents Sea became availabe in 1966, when the first satellite images were made.

Since 1970 the Norwegian Meteorological Institut (DNMI) has routinely been creating ice charts which combine satellite, boat and airplane observations (Loeng 1979). Today they are available daily, since the ice conditions are still important for shipping routes through the Barents Sea.

Additionally, sea ice receives growing attention because of its role in climate. Appart from providing information about climate change by long term observations of ice extent, thickness and volume; sea ice can have an influence on the climate itself. For example through the well-known ice-albedo-feedback and due to its role in the production of dense surface water, which is important in driving the thermohaline circulation. The ice extent in the Barents Sea is discussed to depend on both the wind conditions (e.g. Fang and Wallace 1994, Kimura and Wakatsuchi, 2001) and the ocean currents (e.g. Bengtsson et al. 2004). In addition the air temperature, precipitation and cloud cover influence the ice extent (Vinje 2001). In numerous publications a decreasing trend in the sea ice extent or volume in the Barents Sea is reported (e.g. Maslanik et al.1996, Walsh and Chapman 2001, Kvingedal, Sea-Ice Extent and Variablility in the Nordic Seas, 1967–2002 submitted to Journal of Climate 2005 (hereinafter refered to as Kvingedal, submitted manuskript, 2005)). Also large-scale atmospheric patterns, such as the North Atlantic Oscillation (NAO) and the Arctic Oscillation (AO) are known to influence the Barents Sea (e.g. Dickson et al. 2000, Krahmann and Visbeck 2003, Liu et al. 2004). Not only has the atmosphere the possibility to influence the ocean, also effects of the ocean and its sea ice cover on the atmosphere needs to be taken into account when discussing sea ice variability (Vinje and Kvambekk 1991, Guest et al. 1995, Deser et al. 2000, Wu et al. 2003). Here, the connections between the wind stress field and the sea ice in the Barents Sea is investigated on interanual time scales.

It is further discussed whether the wind stress field is governed by the influence of large scale pattern or rather by local processes. To do this and because also the wind field outside the Barents Sea may have an influence on this area (e.g. through its influence on ocean currents, Ingvaldson et al. 2004) also the wind stress field over the whole Nordic Seas is analysed.

Special attention is given to Storfjorden, a "fjord" located between the east coast of Spitsbergen and the islands Edgeøya and Barentsøya (see Figure 2). It contains frequently a latent heat polynya during winter, opening under strong northerly winds (Vinje and Kvambekk 1991). In addition to the fjord mouth in the south, it is connected to the Barents Sea by two shallow sounds (Heleysundet and Freemansundet) in the northeast. Polynyas are areas of open water in an ice-covered surrounding under freezing conditions (WMO 1972). They can either be formed by warm ocean currents (sensible heat polynyas) or by strong winds driving the ice away from a coast (latent heat

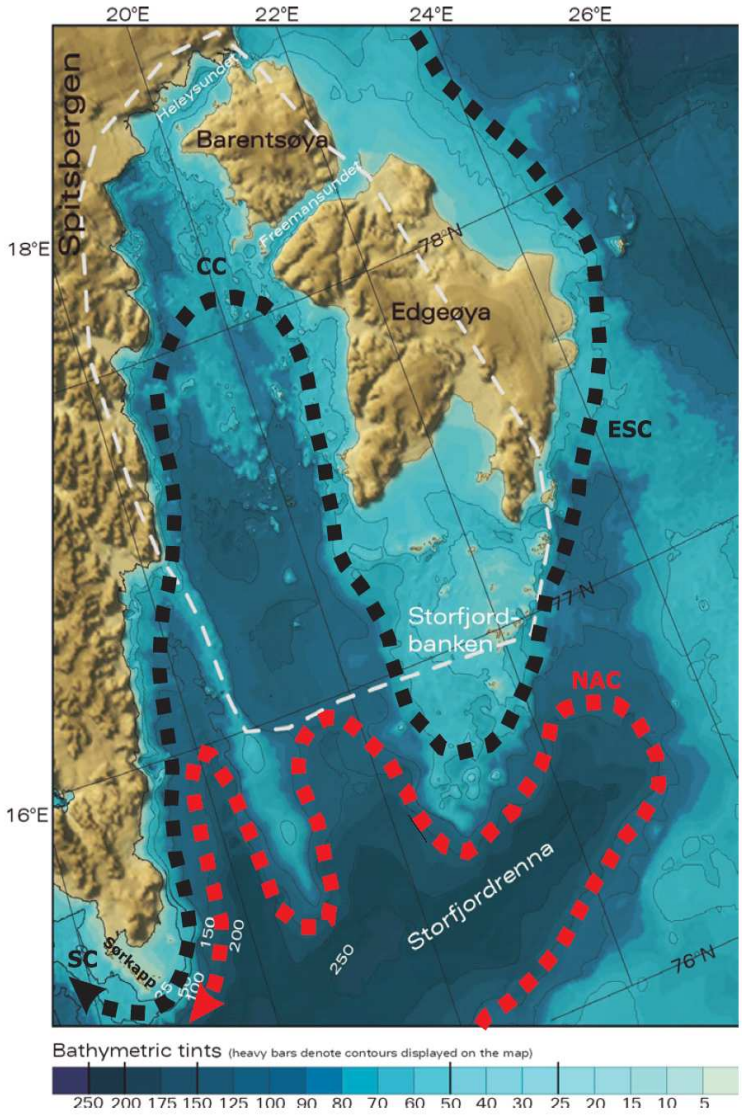

Figure 2: Bathymetry of the Storfjorden area. From Skoseth et al. (2005).

polynyas) (Smith et al. 1990). Latent heat polynyas are known to produce high amounts of ice. Due to the insulating effect of ice much more freezing occurs in areas of open water under freezing conditions (Smith et al. 1990). Since sea water ejects salt while freezing, latent heat polynyas are known to be important for the production of brine water (e.g. Cavalieri and Martin, 1994). The Barents Sea contributes considerably to the maintenance of the arctic halocline, because it is relatively saline (Steele et al. 1995, Windsor and Björk 2000). Storfjorden is assumed to be one of the places most important for the production of brine- enriched shelf water (BSW) in the Barents Sea

(Quadfasel et al. 1988).

The connections between the wind stress and the sea ice cover is investigated around Storfjorden to find a physical explanation for the annually varying ability of the polynya to open and to close. Haarpaintner et al. (2001) and Skogseth et al. (2004) adjusted the modelled polynya width to the width found through the analysis of satellite images and show that the factors necessary for this differ from year to year.

Section 2 presents the data sets used and the methods applied. In Section 3.1 the wind stress field over the Nordic Seas is displayed together with the correlations with the NAO, in Section 3.2 the connections between the wind stress field and the ice extent is investigated and in Section 3.3 presents the modelled total ice production for the years 1970 to 2004 is presented. The discussion follows in Section 4 and the conclusions are presented in Section 5.

2 Data and methods

2.1 Wind stress

The wind stress $\vec{\tau}$ is the transfer of momentum from the atmosphere to the surface (Apel, 1987). It was calculated from the surface wind by the Institute of Marin Research (IMR), Bergen, using:

$$\vec{\tau} = \rho_a C_d \left|\vec{U}_{10}\right| \vec{U}_{10} \tag{1}$$

Here $\vec{\tau}$ is the wind stress vector, ρ_a is the density of air, C_d is the drag coefficient for neutral stability and $\vec{U}_{10}$ is the wind at a height of 10m above the surface. The wind stress is split into its eastward and northward components, τ_x and τ_y respectively.

The magnitude of the wind stress $|\vec{\tau}|$ can be calculated by

$$|\vec{\tau}| = \sqrt{\tau_x^2 + \tau_y^2} \tag{2}$$

It is important to remember that equation 2 is a nonlinear operation. Therefore it makes a difference if the time mean of wind stress magnitudes or averaged components $\overline{\tau_x}$ and $\overline{\tau_y}$ are calculated. In the first case the result is the averaged magintude of the wind stress, in the second case also the shift in direction has an influence. Here the wind stress magnitude is computed from the averaged components $\overline{\tau_x}$ and $\overline{\tau_y}$.

2.1.1 Wind stress curl

The vertical component of the rotation of the wind stress curl (the "wind stress curl") is defined by equation:

$$\nabla_z \times \vec{\tau} = \frac{\partial \tau_y}{\partial x} - \frac{\partial \tau_x}{\partial y} \tag{3}$$

The differentials $\frac{\partial \tau_y}{\partial x}$ and $\frac{\partial \tau_x}{\partial y}$ are replaced here by central differences, therefore the wind stress curl at each point is calculated from the wind stress at the four neighbouring points. This yields to wind stress curl values at the same grid points at which the wind stress is defined. Because the differentials are approximated by differences the average curl results in the same if it is calculated from the mean components or taken over a time series of wind stress curl. This applies also to the wind stress divergence.

2.1.2 Wind stress divergence

The wind stress divergence is defined by:

$$\nabla_H \cdot \vec{\tau} = \frac{\partial \tau_x}{\partial x} + \frac{\partial \tau_y}{\partial y} \tag{4}$$

Here as well central differences are used.

2.1.3 Wind stress and sea ice

The most obvious connection between the wind stress and the sea ice is the ice transport described by the Nansen-Ekman drift law (Nansen 1902). It states that the sea ice drifts with an angle of about 30^o to the right of the surface wind direction (Figure 3). It follows, that a positive (cyclonic) wind

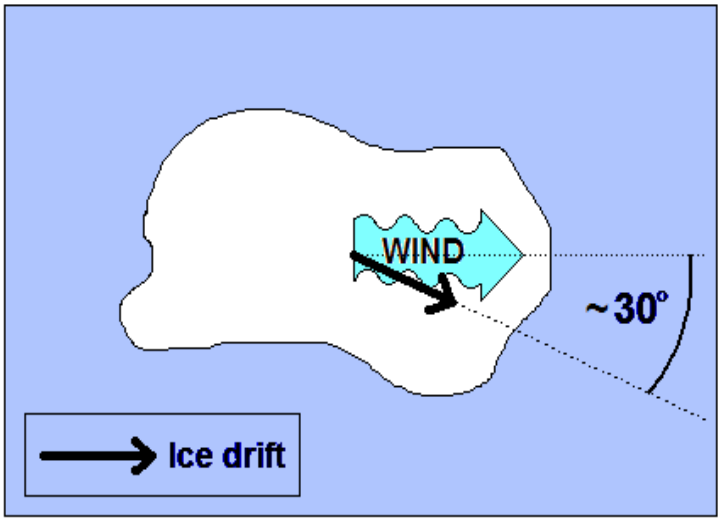

Figure 3: Schematic picture of the influence of wind stress on the ice drift.

stress curl and a positive wind stress divergence lead to a divergence of sea ice (Läpperanta, 2005; Bailey et al. 2004). This is shown shematically in Figure 4.

Another connection between the wind stress and the sea ice is observed in the presence of low pressure systems. As will be shown in Section 3.1 they show high wind stress curl and divergence values. A low pressure system entering an ice covered region will in most cases lead to a reduction in concentration of ice and ice floe size. Hence the melting is increased if the water temperature is above the freezing point (Holt and Martin 2001). Therefore the position of the storm tracks can be important for the sea ice extension in spring. Additionally, low pressure systems are often connected to the advection of warm air into the subpolar and polar regions (Overland and Pease, 1982). This can as well lead to enhanced melting or reduced freezing. Further, also the ice cover can influence the wind stress field: Because the heat fluxes to the atmosphere over an ice covered sea are much smaller than over open water (Deser et al. 2000), one may assume that more low pressure systems occur when the ice extent is reduced.

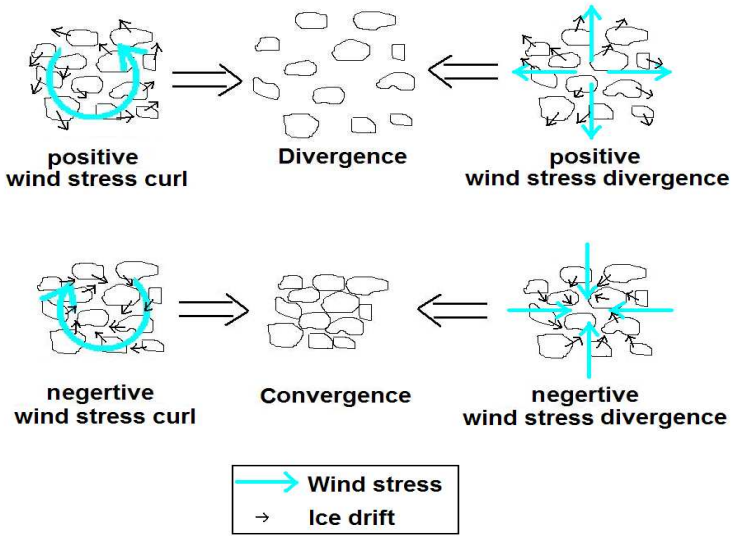

Figure 4: Schematic picture of the influence of wind curl and wind stress divergence on the ice drift.

Wind stress is observed to be lower over ice covered areas eventhough the surface roughness is often higher, because of a lower boundary layer caused by smaller heat fluxes due to a lower surface temperature (Davidson et al. 1992, Guest et al. 1995). However, according to Wu et al. (2004), also the local pressure field can be influenced by the changes of the atmospheric boundary layer and would then be also reflected in the data used here. Since the wind stress fields used here are not measured directly but calculated from pressure fields without paying attention to these processes (see Section 2.3), they are neglected. The main focus will be given to the influence of the atmosphere on the sea ice. This is supported by the results of Fang and Wallace (1994) and Yi et al. (1999) who found examles for higher correlations between sea ice and atmospheric pressure were higher when the atmosphere was leading.

On interannual time scales also the water temperature itself and the position of the Polar Front can be important for the ice extent in the Barents Sea (Ådlandsvik and Loeng 1991). The water temperature is also influenced by the wind field over the Barents Sea. Ingvalson et al. (2002) found an increased inflow of relatively warm Atlantic Water into the Barents Sea when southwesterly winds prevail at its entrance.

2.2 Methods

2.2.1 Winter mean

Since the ice data have a much coarser temporal resolution than the wind stress data, usually only the winter mean of the different wind stress parameters is considered. Winter refers here to the months December to March (DJFM) for the ice index for the central Barents Sea (I_w, see Section 2.4.2) and the NAO winter index, since the strongest wind stresses are observed during these months. For the comparison with the polynya model, the mean over the period from December to April (DJFMA) is used. In this way a bigger fraction of the freezing period for Storfjorden is covered, which usually lasts from mid November to mid May. The ice index for the whole Barents Sea (I_{BKB}, see Section 2.4.3) covers only the month December to February (DJF), therefore also the wind stress data are only averaged over this time period for comparison with I_{BKB}. The time average of the wind stress components, the wind stress curl and the wind stress divergence is calculated from the time series of each variable at every grid point. The mean wind stress magnitude is calculated from the averaged wind stress components, as explained in Section 2.1. The year given for each winter always refers to the year of January, e.g. winter (DJFM) 2004 means December 2003 to March 2004.

2.2.2 Spearman Rank correlation

To estimate the connections between the different parameters, the Spearman Rank correlation coefficient (r_s) is calculated, if the time series start in 1970 or earlier. For this, a Matlab program based on the routine from Press et al. (1992) is used. The Spearman Rank correlation is used, because it is more robust than a usual correlation and can handle not gaussian distributed data. It provides advantages, when regressions between two variables are monoton but not linear (Sachs, 1992). It can be calculated by

$$r_s = 1 - 6 \sum \frac{d^2}{N(N^2 - 1)} \tag{5}$$

where d is the difference in statistical rank between corresponding variables and N is the length of the time series (Weisstein, 1999). The confidence level is estimated following Press et al. (1996).

To prevent any loss of information the Spearman Rank correlation is not used for the comparison between the opening an closing factors of the polynya model and the wind stress fields. The correlations and the significance level here are calculated by a correlation computed through the Matlab program corrcoef, which is based on the equation:

$$r = \frac{\sum xy - n\overline{x}\,\overline{y}}{\sqrt{(\sum x^2 - n\overline{x})(\sum y^2 - n\overline{y})}} \tag{6}$$

Boths kinds of correlations are denoted to be significant here, when they exceed the 95 % confidence level.

2.3 The Hindcast data set

The wind stress data are available for the period from 01.01.1955 to 19.08.2004. They were provided by the Institute of Marine Research, Bergen, (IMR) and were derived from a hindcast data set of the 10m surface winds from the Norwegian Meteorological Institute (DNMI). The DNMI has calculated the surface winds with a two layer boundary layer model from the geostrophic wind derived from surface pressure maps as described by Reistad and Iden (1998). They assumed neutral stability and used Charnock's relation to compute the roughness. Therefore the wind calculations are not realistic for land and sea ice.

It is difficult to estimate how this influences the long time wind stress means used for comparison with the sea ice data, especially because the wind stress is proportional to C_D, and to the square of the surface wind (see Equation 1). This means that a too high roughness leads to a higher wind stress, but at the same time to a lower surface wind resulting in a lower wind stress. Additionally, the usually more stable stratification over sea ice relative to open water influences C_D (Davidson et al. 1992). In genearl the correct roughness over the marginal ice zone is difficult to estimate, because it can change a lot on small spatial scales due to changes of the kind of ice (Davidson et al. 1992). The parametrisation with a C_D for neutral stability and Charnock's relation does not reflect the conditions over sea ice correctly and is probably causing some error in the wind stress estimation. However, the influence of synoptic scale weather systems on the wind stress field should be dominant.

The methods the DNMI used to obtain these pressure fields changed with time: From 1955 to 1981, the surface pressure maps were obtained by a Cressman analysis (Cressman 1959) of observations. Afterwards, the operational global analysis of the European Centre for Medium Weather Forecast (ECMWF) was used until May 1987. Then a weather prediction model of DNMI was used, integrated first on a 150km grid and from May 1990, on a 50km grid. From the 1 January 1996 this model was replaced by the High Resolution Limited Area Model (HIRLAM) (Reistad and Iden, 1998).

2.3.1 Area

The area is chosen so that in addition to the Barents Sea the whole region of the Greenland, Island and Norwegian Sea (GIN Sea), the Fram Strait and the area around Svalbard is covered (see Figure 5). The data are provided on a 75km grid. To interpolate the data from the original 150 or 50km grid the DNMI used a linear interpolation. The results are usually only presented for ocean regions, because the calculation of the wind stress is not adjusted to the changed boundary conditions over land (see Section 2.1). Because the handling of an rectangular grid is more convenient, data points on land are not totally excluded.

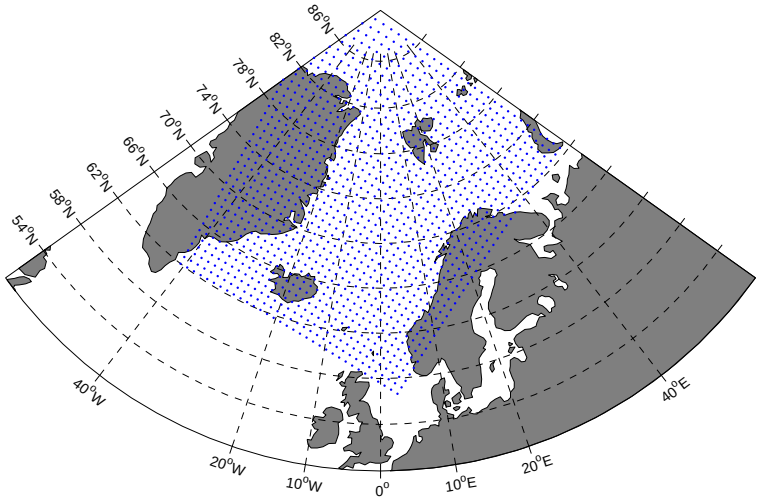

Figure 5: Area and Grid used.

2.3.2 Data quality

Because of changes in the methods to obtain the pressure fields and in the observation density, inhomogenities are likely to occur. In order to improve the data quality the wind calculations were tuned by the DNMI, by adjusting them to time series measured by weather stations close to the grid point. This was mainly done close to the Norwegian coast. Nevertheless, some changes of the wind stress seem to arise from differences in the computation rather than from a real change. Especially northwards of 78^oN and in the whole area of Greenland, "jumps" in the time series occur, as can be seen in Figure 6. These shifts occure mainly during the 1980s, the largest one is most probably caused by the change from the Cressman analysis to the ECMWF analysis in 1981, but also the change to the model of DNMI in 1987 seems to have an effect.

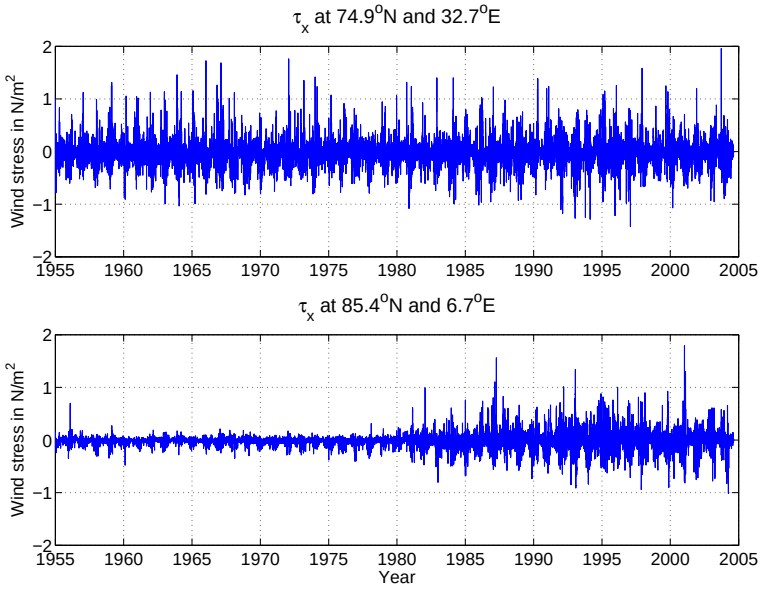

Figure 6: Time series of τ_x (in N/m^2) at two different locations. Upper panel: At 74.9^oN, 32.7^oE in the central Barents Sea. Lower panel: At 85.4^oN, 6.7^oE north of the Fram Strait. For the positions see Figure 7.

To emphasize the extent of these shifts, data from the 1990s are compared with those from the 1970s. The normalized difference between the variance from 1990 to 1999 and 1970 to 1979 is taken; the same is also done for the mean. For τ_x this is done by

$$\frac{var(\tau_x)_{1990s} - var(\tau_x)_{1970s}}{var(\tau_x)_{1990s} + var(\tau_x)_{1970s}} = \text{Normalized difference of variance} \quad (7)$$

$$\frac{|\overline{\tau_x}_{1990s}| - |\overline{\tau_x}_{1970s}|}{|\overline{\tau_x}_{1990s}| + |\overline{\tau_x}_{1970s}|} = \text{Normalized difference of mean} \quad (8)$$

and analogous for the other wind stress parameters. The result for τ_x is shown in Figure 7, for tτ_y in Figure 8, for the wind stress curl in Figure 9 and for the wind stress divergence in Figure 10.

Figure 7 to 10 show clearly that the biggest differences occur in the north of the analysed area and over Greenland. The differences are also more pronounced for the variance than for the mean: The areas where the mean in the 1990s are twice as high as in the 1970s is nearly identical with that where the variance is five times as high. The lower values of variance in the 1970s is most probably due to the coarser grid used by the less advanced models, in which some synoptic phenomena including fronts and polar lows are not well resolved. It can be assumed, that the quality in the region where also the mean value is affected is not sufficient before the 1982. Eventhough

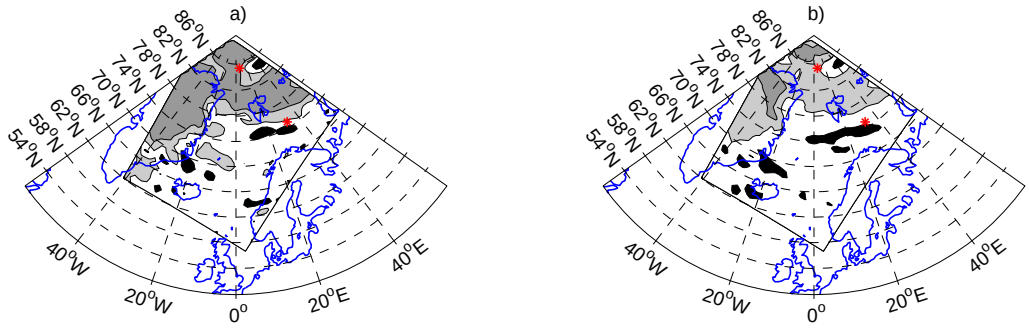

Figure 7: Normalized difference between (a) the variance of τ_x in the 1990s and the 1970s and between (b) the magnitude of the mean of τ_x in the 1990s and the 1970s. Light grey shadings indicate a value twice as high in the 1990s as in the 1970s, dark grey shadings one five times as high. Areas the value is higher during the 1970th are marked in black. The red stars mark the positions of the time series shown in Figure 6.

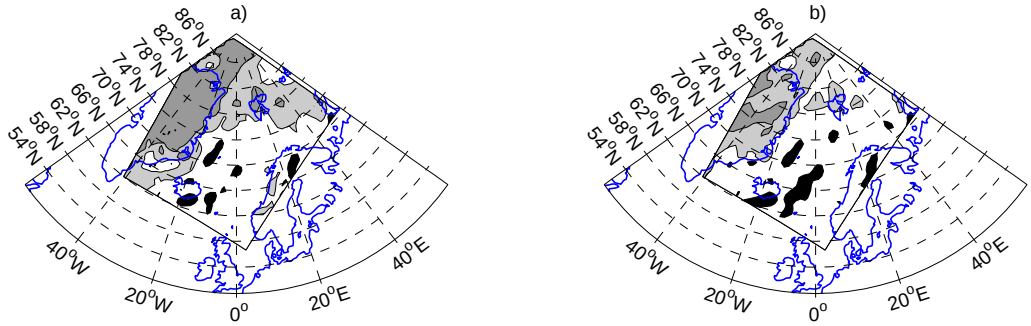

Figure 8: As in Figure 7 but for τ_y.

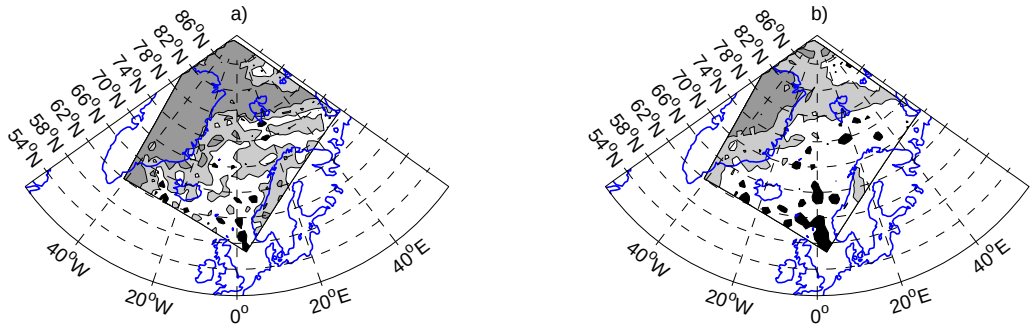

Figure 9: As in Figure 7 but for the wind stress curl.

Walsh et al. (1996) find a decrease of sea level pressure and an increase of their vorticity index in an presumably homogenous data set over the Arctic

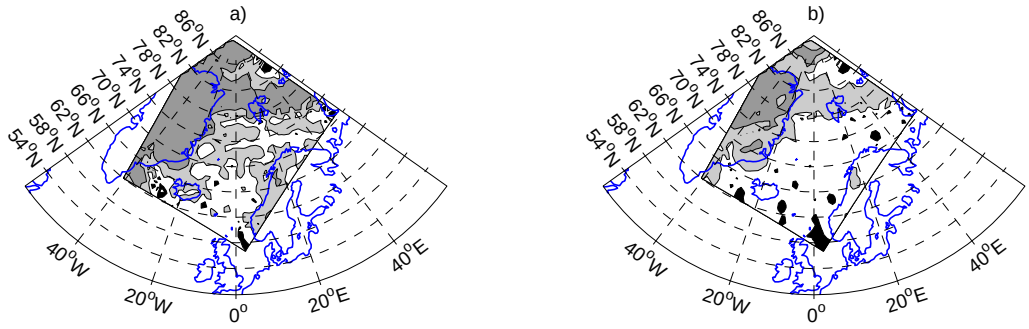

Figure 10: As in Figure 7 but for the wind stress divergence.

Ocean in the 1980s (including to "jumps" in 1981 and 1987, see their Figure 6), the shift in 1981 found in the data set used here is rather caused by low data quality. Reasons for that are:

- The differences occur only regionally and not in the whole area.
- The observation in this region are known to be sparse, therefore the improvement of numerical models during the last decades will have affected the data quality in such areas.
- Large parts of this region are at least periodically covered by sea ice. This is not taken into account in the hindcast calculation (see Section 2.1).

Comparing Figure 7 and 8 to Figure 9 and 10 shows that the differences cover a larger area for the wind stress curl and the wind stress divergence than for the wind stress components and the absolute wind stress. The cause for this is most probably that the curl and the divergence are calculated from the gradient of several grid points of the wind stress components (see Section 2.1). Hence they are more sensitive to mistakes caused by a coarser grid.

2.4 Sea ice

The sea ice extent is is defined as the area covered with ice of any type or concentration (Kvingedal, submitted manuscript, 2005). It varying on all time scales due to atmospheric and oceanic influences. In the Barents Sea both seasonal and interanual variations are large (Vinje and Kvambekk 1991).

2.4.1 Sea ice observations

Regular information about the sea ice extent in the Barents Sea is available from 1966, when observations by weather satellites started (see Loeng, 1979). From 1970 the DNMI published ice charts regularly, combining information from satellite data, boat and airplane observations (Loeng, 1979). The ice indices described in Section 2.4.2 and 2.4.3 start therefore from this year. Indices of ice extent are used, because the extent is the property of the sea ice, which can be monitored most reliably by satellites. They are all derived from ice maps produced by the DNMI. These maps are based on observations by boats and airplanes as well as NOAA/AVHRR and DMSP, SSM/I satellite data. From September 2003 on, QuickScat sea wind data were included for the ice edges.

To estimate the size of smaller structures in the ice such as the polynya in Storfjorden their resolution is not sufficient. Therefore higher resolution satellite images have to be used. This is described in more detail in Section 2.4.4.

2.4.2 The Barents Sea Ice Index by Harald Loeng (I_w)

The Barents Sea winter Ice Index (I_w) is computed by the IMR, Loeng (pers. comm.). It is defined by

$$I_w = -\int_{winter} (\text{ice covered area south of } 76^o N) dt \tag{9}$$

in a zone between 25^o and 45^oE (Loeng 1979, Ådlandsvik 1991).

Here I_w is used for comparison with the wind stress and the output of the polynya model for Storfjorden. It is shown in Figure 11a. In Figure 12 an ice map from DNMI is shown together with the area covered by I_w. This area in the central region of the Barents Sea was chosen to exclude the influence of land (Loeng, 1979).

2.4.3 The indices of ice extent by Børge Kvingedal

The index of sea ice extent for the Barents Sea I_{BKB} by Kvingedal and Sorteberg, Atmospheric forcing on Barents Sea Ice, submitted to Journal of Climate (2005) (hereinafter refered to, Kvingedal and Sorteberg, submitted manuscript, 2005) can be seen in the middle panel of Figure 11. It is based on the ice extent and the fraction in a region between 85^oN and 20^oE and 80^oE (see Figure 13) during December to February (DJF).

With the same method, Børge Kvingedal (pers. comm.) also derived an index for the region south of Storfjorden (I_{BKS}). It is defined on an area south of 78^oN and between 12^oE and 31^oE and can be seen in the lower

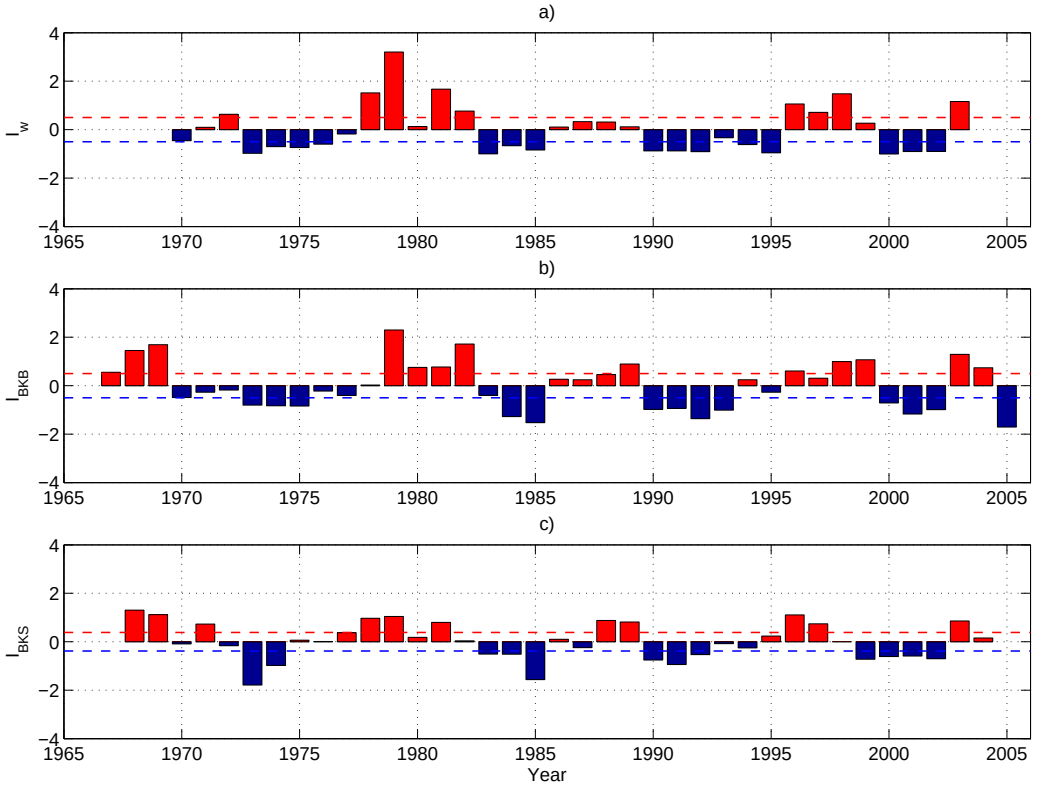

Figure 11: a)I_w for the years 1970 - 2003. b) I_{BKB} for the years 1967 - 2005. c) I_{BKS} for the years 1968 - 2004. All indexes are normalized. The broken lines show the $\pm 1/2$ standard deviation for each index.

panel of Figure 11. The area is shown in Figure 13. To agree better with the freezing season in Storfjorden, I_{BKS} covers the months December to April (DJFMA). I_{BKB} and I_{BKS} are available since 1967 and 1968, respectively, but for the comparison with the wind stress field only the years since 1970 (incl. December 1969) are used to have the same starting year for all indices.

2.4.4 The polynya model for Storfjorden

At Storfjorden, located between Spitsbergen, Edgeøya and Barentsøya (see Figure 2), a latent heat polynya occurrs frequently in winter (Vinje and Kvambekk, 1991). For this polynya a numerical model was developed by Haarpaintner et al. (2001) and further improved by Skogseth et al. (2004), to compute the polynya size, the total ice volume produced and the production of BSW. It uses meteorological data from Hopen Island as input. Because Hopen Island is located southeast of Storfjorden, the temperature is adjusted by subtracting 3.5^{o}C. This value was estimated by comparing the

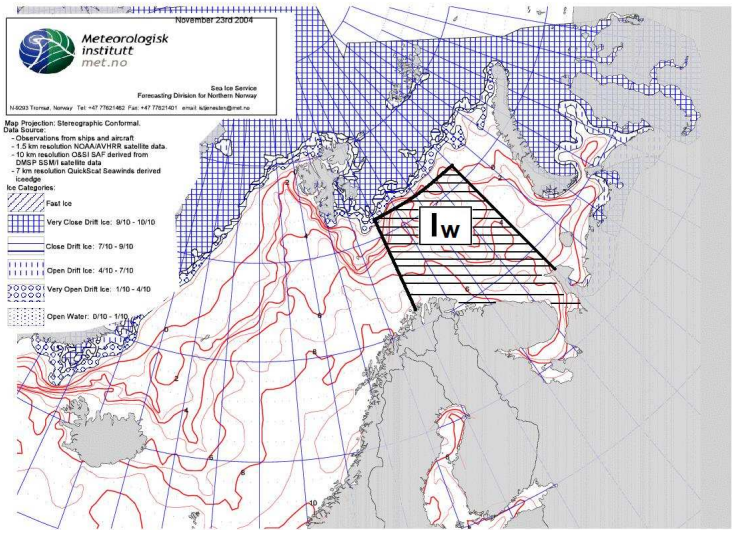

Figure 12: Ice map from DNMI on 23 November 2004. The area over which I_w is defined is highlighted.

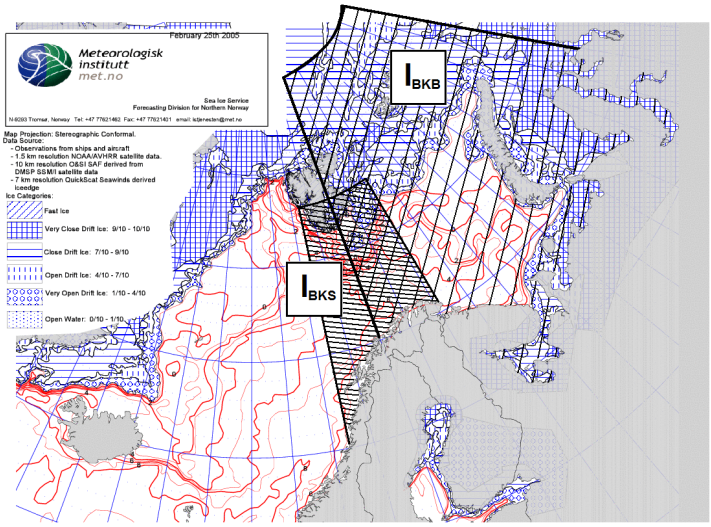

Figure 13: Ice map from DNMI on 25 February 2005. The areas defining I_{BKB} and I_{BKS} are highlighted.

temperature at Hopen Island to measurements from automatic weather stations at Edgeøya and Kapp Dufferin (Skogseth et al. 2004). The wind speed and direction from Hopen Island are not adjusted, because due to strong influences of the local topography, the measurements at Edgeøya and Kapp Dufferin are not necessarily more representative for Storfjorden (Skogseth et al. 2004).

The polynya model devides between different ice classes:

Frazil ice is newly formed ice which consists of "fine spicules or plates of ice suspended in water" (WMO, 1972). For the polynya model areas with frazil ice are included in the open water area.

Thin ice consists of a newly formed thin ice layer or small ice floes. In the polynya model it is included in the polynya area.

Fast ice is sea ice which is attached to the shore and does not drift (WMO, 1972).

Pack ice includes any kind of sea ice which is not fast ice (WMO, 1972). For the polynya model it also excludes thin and frazil ice.

The mass of total ice production (T_{is}) is calculated by for every time step by

$$\Delta T_{is} = \rho_f \Delta V_f + \rho_i \Delta V_i \tag{10}$$

(Skogseth et al. 2004), where $\rho_f = 950 kgm^{-3}$ is the frazil ice density (Martin and Kaufmann, 1981), $\rho_i = 920 kgm^{-3}$ is the density of ice from continuous grows. ΔV_f is the produced volume of frazil ice and ΔV_i the one produced by continuous ice grows for every time step (Skogseth et al. 2004).

The frazil ice production occurs in areas of open water in the polynya and in leads in thin, fast and pack ice. ΔV_f is calculated by

$$\Delta V_f = \Delta h_f (A_0 + P_{fp} A_{fp} + P_t A_t) \tag{11}$$

where A_0 is the area of open water in the polynya, A_{fp} is the area of fast and pack ice, $P_{fp} = 0.01$ is the fraction of fast and pack ice, which is covered by leads, A_t is the area of thin ice and $P_t = 0.25$ the coresponding fraction covered by leads (Skogseth et al. 2004).

Δh_f is the equivalent thickness of frazil ice, with

$$\Delta h_f = \frac{F_{net}}{\rho_f L_s} \Delta t \tag{12}$$

where F_{net} is the heat flux over open water and $L_s = 234.1 kJkg^{-1}$ is the latent heat of fusion for sea ice (Skogseth et al. 2004).

The continuous ice grows ΔV_i takes place under thin, fast and pack ice and is calculated by

$$\Delta V_i = \Delta H_{fp}[(1 - P_{fp} A_f p)] + \Delta H_t[(1 - P_t) A_t] \tag{13}$$

where ΔH_{fp} and ΔH_t are the ice grows in meter for fast and pack ice and thin ice, respectivly. It is calculated by the differential numerical ice growths algorithm (Maykut 1986, Haarpaintner et al. 2001)

$$\Delta H = \frac{0.129}{2H + 13.1h_s + 0.168}\Delta\Theta \tag{14}$$

where H is the ice thickness in meters, $\Delta\Theta$ is the increase in cumulative freezing degree days in Kelvin second and h_s is the snow thickness, which is assumed to increase lineary with $1.2\ mm\ d^{-1}$ for fast and pack ice (ΔH_{fp}) and is neglected for thin ice (ΔH_t) (Skogseth et al. 2004).

In contrast to the model runs by Haarpaintner et al. (2001) and Skogseth et al. (2004) the salt release and the volume of BSW are not calculated here, because the calculation requires knowledge of the initial salinity in Storfjorden in the autumn before each modelled year. These data are not available regularly before 1998.

The polynya width $W_{p,n}$ (width of the area with open water and thin ice) at a time n is calculated by

$$W_{p,n} = W_{p,n-1} + F(\Phi_n - \Phi_0)B_1U_n cos(\Phi_n - \Phi_0)\Delta t \tag{15}$$

where $B_1 = 0.02$ is the ice drift factor, U_n is the 10m wind speed at Hopen, Φ_n is the wind direction, $\Phi_0 = 10^o$ is the most effective wind direction for opening the Storfjorden polynya (Haarpaintner et al. 2001) and $\Delta t = 6h$ is the time step (Skogseth et al. 2004). The initial polynya width is set to zero and the polynya width cannot become smaller than zero (Skogseth et al. 2004). $F(\Phi_n - \Phi_0)$ is an opening or closing factor, the polynya is assumed to open, for $-90^o < \Phi_n - \Phi_0 < 90^o$ and to close for $90^o < \Phi_n - \Phi_0 < 270^o$ (Skogseth et al. 2004). The dimension of the polynya perpendicular to the width across Storfjorden is set constant to 48km to calculate the area (Haarpaintner et al. 2001). For the complete model describtion see Skogseth et al. (2004).

The polynya width is also estimated from satellite images. In Haarpaintner et al. (2001) and Skogseth et al. (2004), European Remote Sensing satellite (ERS-2) syntitic aperature radar (SAR) images where used for the winters 1998 to 2002. For 2003 and 2004 Envisat advanced syntitic aperature radar (ASAR) Quicklook images from the EOLI Catalogue were used. An example for that can be seen in Figure 14. Here open water and thin ice where not distinguished from each other because of the coarser resolution of the images.

The modelled polynya is adjusted to the size of the SAR-estimated polynya by the opening and closing factors ($F(\Phi_n - \Phi_0)$) for each winters. For the winters 1998-2001 these factors can be found in Skogseth et al. (2004). The

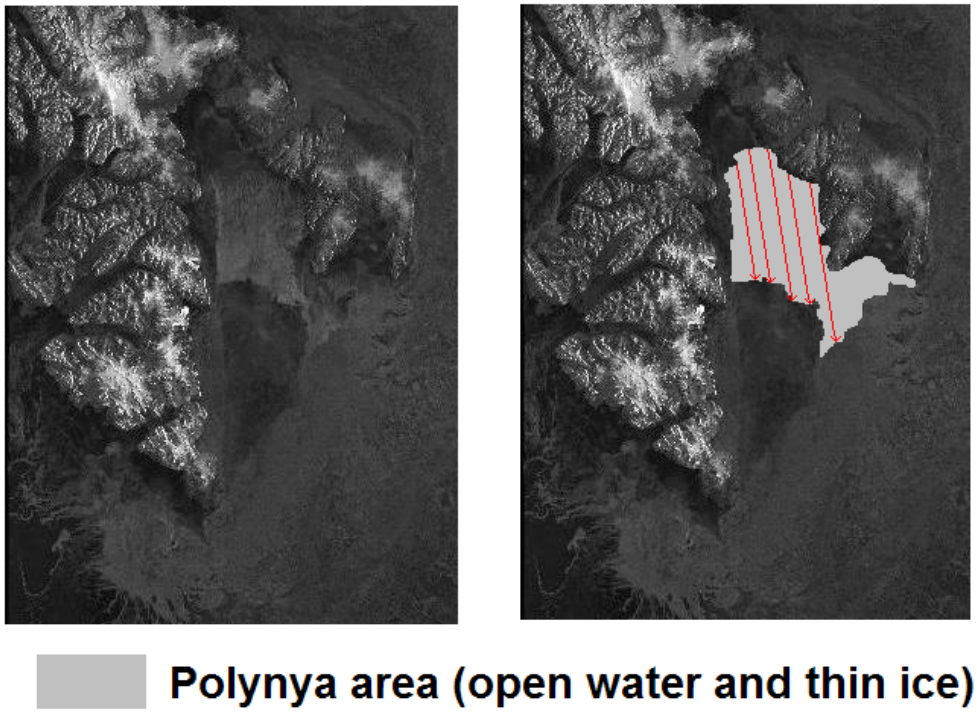

Figure 14: Envisat ASAR Quicklook picture of the Storfjorden area from the EOLI Catalogue (http://muis-env.esrin.esa.it:8080/servlets/template/welcome/entryPage2.vm) from 4 April 2003. In the right panel the polynya area (open water and thin ice) is marked. The arrows indicate how the polynya width is estimated.)

factor for 2002 was calculated by Skogseth (pers. comm.). For 2003 and 2004 they are presented in Section 3.3. In the following the opening and closing factors are denoted by OF and CF, respectivly.

CF is about 15 times higher than OF, because of the production of new ice in the open water area (Haarpaintner et al. 2001). Additionally, the factors vary interannually, presumably because of different amounts of ice and ice compactness in Storfjorden and in front of the fjord mouth. This will be investigated further in Section 3.3.

2.5 NAO index

To estimate the influence of the large-scale atmospheric circulation on the wind stress field over the Barents Sea and the Nordic Seas it is compared to the winter (DJFM) NAO index (following just denoted "NAO index"). The NAO index from http://www.cru.uea.ac.uk/cru/data/nao.htm is used for the

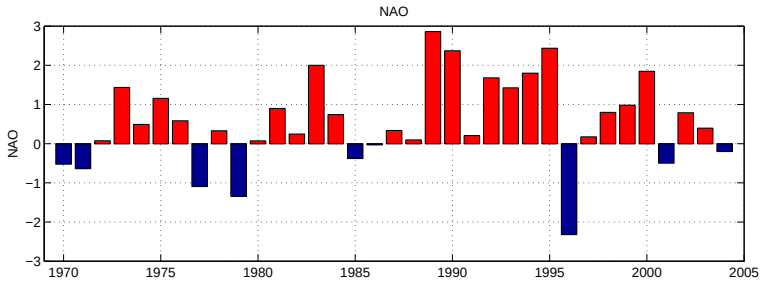

Figure 15: NAO index for the years 1970–2004.

years 1970–1999 and from winter 2000 the update from http://www.cru.uea.ac.uk/∼timo/projpages/nao_update.htm. Both are calculated from the normalized pressure difference between Gibraltar and southwest Iceland, as described by Jones et al (1997). The index is shown in Figure 15.

Since the shortest used time series of ice observations starts in 1970 also the comparison between the wind stress field and the NAO (Section 3.1.3) is just performed from 1970 onwards to prevent confusion and keep the influence of probably erroneous data in the north before 1981 constant. Thus only a period of mainly positive NAO is considered.

2.6 Salinity data in Storfjorden

When sea ice freezes it releases brine water into the ocean. Therfore the total ice production in Storfjorden can be assumed to govern the salinity of the produced BSW, together with the initial salinity of the Arctic Water in autumn (Schauer 1995). The modelled total ice production is compared to the maximum measured salinities from Storfjorden for the years available. The salinity values are measured by CTD (conductivity-temperature-depth) systems on different cruises. Until August 2002 the salinity values can be found in Skogseth et al. (2005). The later values are given in Table 1. They were provided by the Geophysical Institute of the University of Bergen (Ilker Fer, pers. comm.). No salinity measurements were available in the deep water of Storfjorden in 2004 due to severe ice conditions. Most measurements revealed the presence of Brine-enriched shelf water (BSW), which is defined to have a salinity of more than 34.8 psu and a temperature lower than -1.5^{o}C (Schauer 1995). No BSW was found in the years 1989, 1994 and 1995, as can be seen in Figure 16.

Table 1: Maximum salinities in Storfjorden after September 2002

Vessel	Year	Month	Day	Salinity [psu]	Potential temperature [^{o}C]
Håkon Mosby	2002	10	13	35.34	-1.597
Polarstern	2003	03	19	34.98	-1.915
GO SARS	2003	09	08	35.00	-1.82

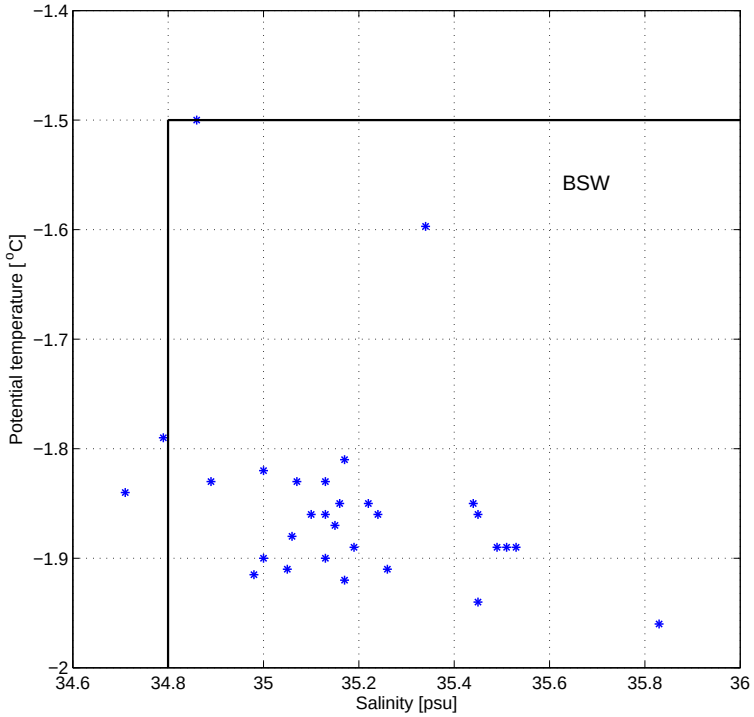

Figure 16: Potential temperature and salinity diagram for the measurements of maximum salinity in Storfjorden.

3 Results

3.1 The wind stress field over the Nordic Seas

By comparing weather maps (Figure 17) to the corresponding fields of wind stress (Figure 18) it is obvious that the surface wind stress roughly follows the isobars. The wind stress curl (Figure 19) and wind stress divergence (Figure 20), are strongest in the presents of low pressure systems or their fronts. One the given Figures, one can for example recognize the low pressure system west of Svalbard to coincide with positive wind stress curl and divergence. Likewise the fronts over the GIN Sea exibit a similar connection. In the

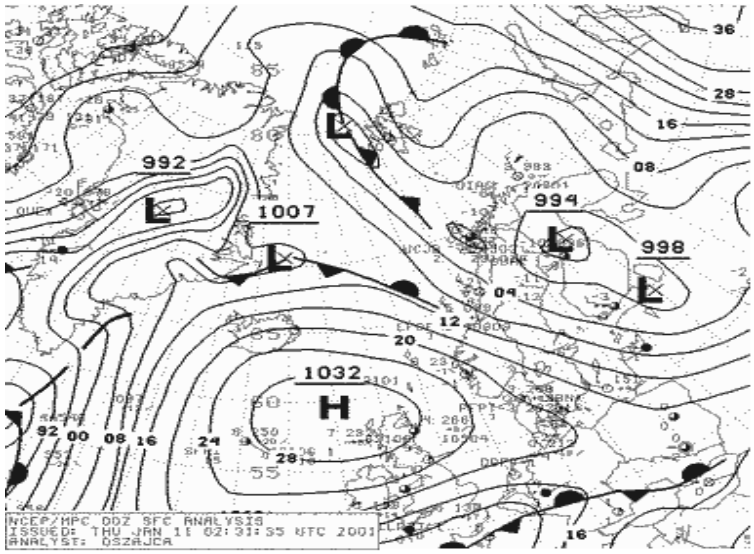

Figure 17: Weather map on 11 January 2001. From National Weather Service, archived at www.wetterzentrale.de.

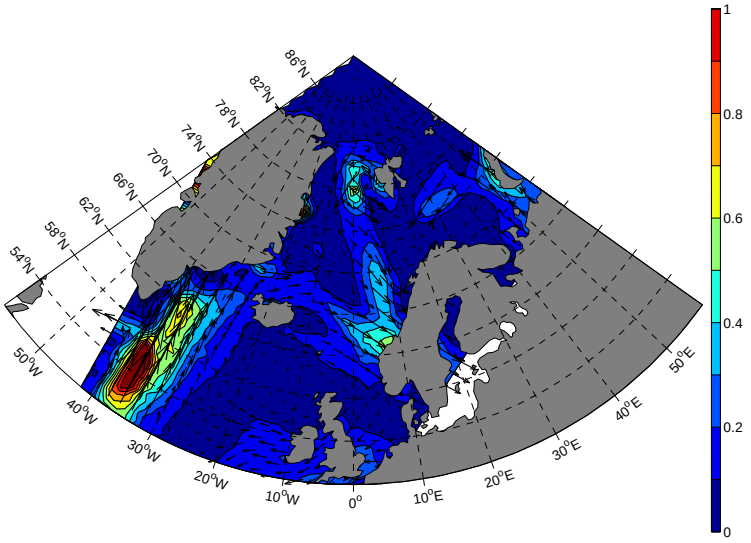

Figure 18: Wind stress field on 11 January 2001. The contours show the magnitude in N/m^2

vincinity of the high pressure system south of Iceland the wind stress curl is mostly negative, while the wind stress divergence displays both, positive and negative values. Conspicuous is also a large positive anomaly of wind stress curl and divergence west of Novaya Zemlya, which is not directly connected to a pressure system but to a cyclonic turn in the wind field.

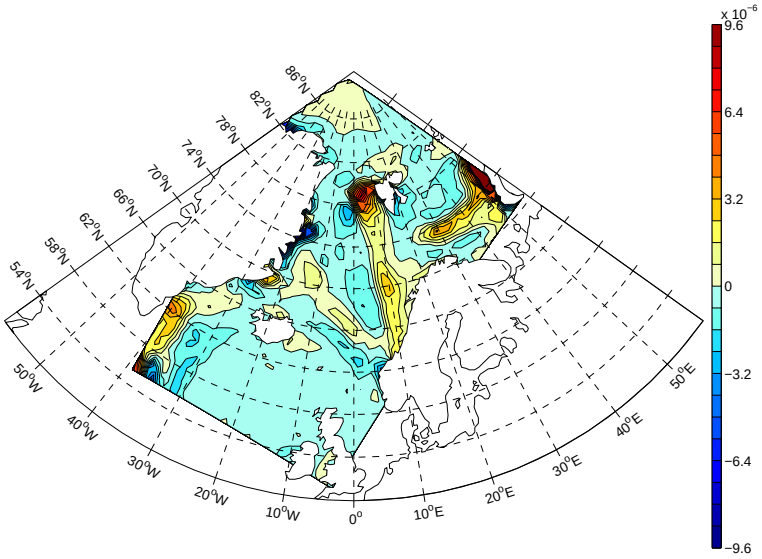

Figure 19: Wind stress curl in N/m^3 on 11 January 2001.

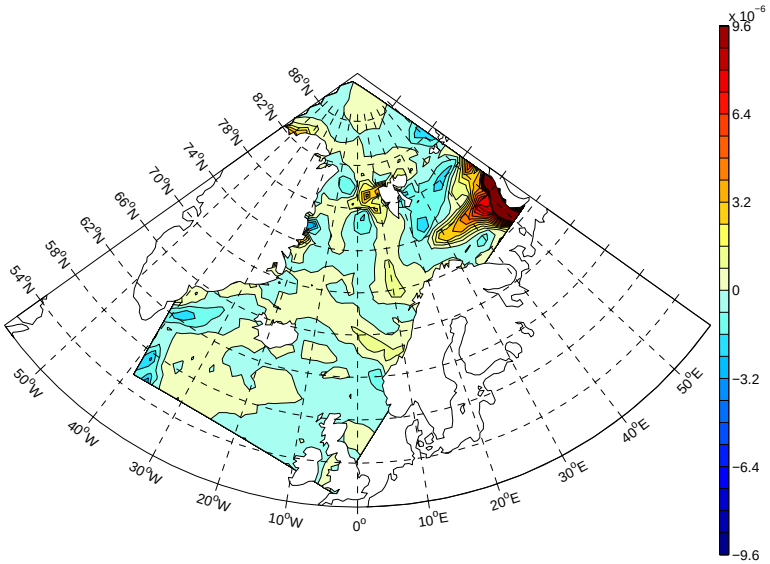

Figure 20: Wind stress divergence in N/m^3 on 11 January 2001.

3.1.1 1970–2003 climatology

The climatological wind wind stress field over the Barents Sea and the Nordic Seas for the years 1970–2003 is shown in Figure 21. In the Barents Sea, a cyclonic rotation can be seen in the mean wind stress field, centred in the Norwegian Sea southwest of the entrance of the Barents Sea. The wind stress magnitude is largest near the coast of Norway and Russia and south of Svalbard while it is rather weak in the central Barents Sea and East of

Svalbard. The wind stress is mainly southerly apart from the area between Svalbard and Franz Josef Land. South about 72^oN the wind stress is mostly westerly, while further north, it becomes easterly. The average wind stress is southwesterly west of the British Islands, over the North Sea and along the Norwegian coast. Strong northeasterly wind stress can be found along the coast of Greenland.

The mean wind stress curl can be seen in Figure 22. In the Barents Sea, it is positive (cyclonic) in the south. In the north, an area of negative (anticyclonic) wind stress curl extents from the east coast of Svalbard eastwards to the west coast of Novaya Zemlya. A small patch of negative wind stress curl is found southeast of Franz Josef Land. Over most parts of the open sea positive wind stress curl is dominant, while areas with negative wind stress curl can be found along the northeast coast of Greenland, east of Svalbard and in small patches around the north coast of the British Islands, along the west coast of Norway and in the Atlantic southwest of Iceland.

In Figure 23, the mean wind stress divergence is shown. In general, it shows the largest values over the Barents Sea. Here, high values of positive wind stress divergence can be found both in the south and in the east, negative wind stress divergence ($\hat{=}$ convergence) prevails in an area east of Svalbard. Also in the southern Barents Sea the wind stress curl and divergence have the same sign, while the maximum of positive wind stress divergence along the coast of Novaya Zemlya is not found for the wind stress curl. Outside the Barents Sea, the wind stress divergence is negative around Iceland, along the east coast of Greenland and in some areas around the British Islands and positive over the biggest part of the Norwegian Sea.

In most areas the mean wind stress curl and divergence show similarities. The biggest differences can be found in the southeastern Barents Sea, where the wind stress divergence is especially high, and southwest of Iceland, where the wind stress curl is positive and the divergence is negative.

3.1.2 Seasonality

Winter

Figures 24–26 show the mean fields of the wind stress, the wind stress curl and the wind stress divergence for the winters (DJFM) of 1970–2004. The fields in winter are generally similar to the climatology, but the magnitudes are higher.

Summer

The mean summer (June to September, JJAS) fields of the wind stress, the wind stress curl and the wind stress divergence are shown in Figure 27- 29. These fields differ from the annual means, and the magnitudes are in general

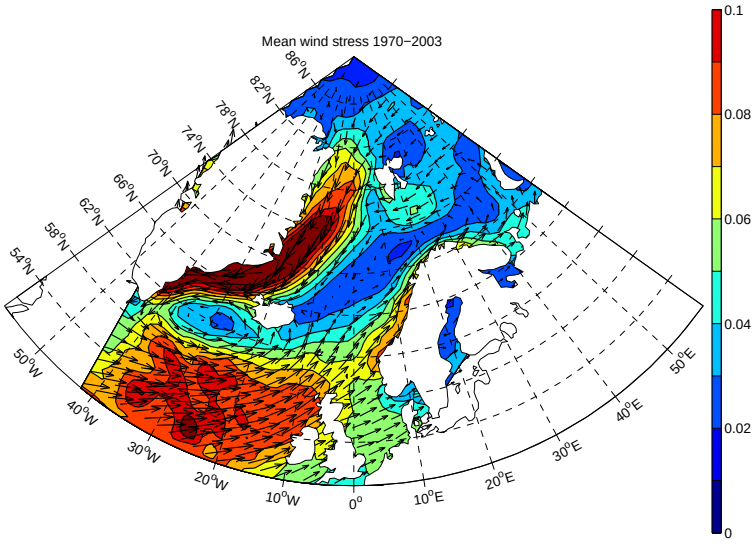

Figure 21: Mean wind stress 1970–2003. Arrows indicate the direction and relative strength of the wind stress, colours the wind stress magnitude in N/m^2.

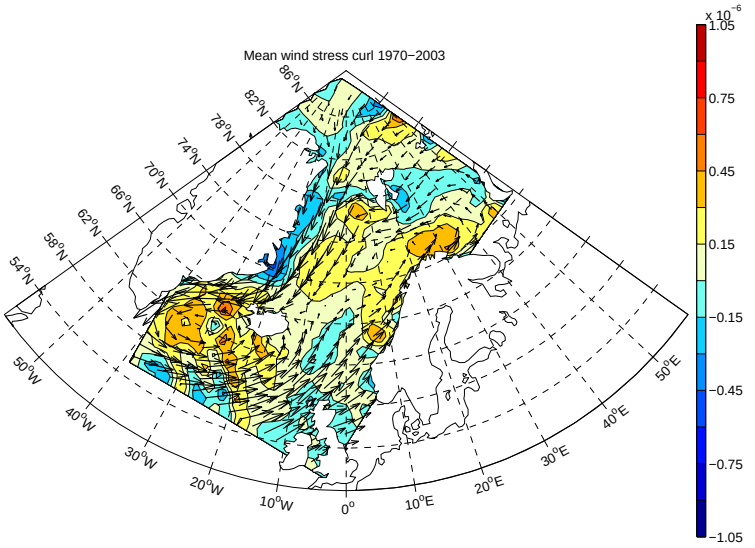

Figure 22: Mean wind stress curl in N/m^3 1970–2003 (colours). Arrows as in Figure 21.

much smaller than in winter. In the Barents Sea, the cyclonic rotation is much weaker during summer and located in the southwestern corner. The wind stress is mostly easterly. The highest wind stress magnitude in summer can be found near the east coast of Greenland and southwest of Iceland in the North Atlantic. The wind stress curl exibits the largest changes in the

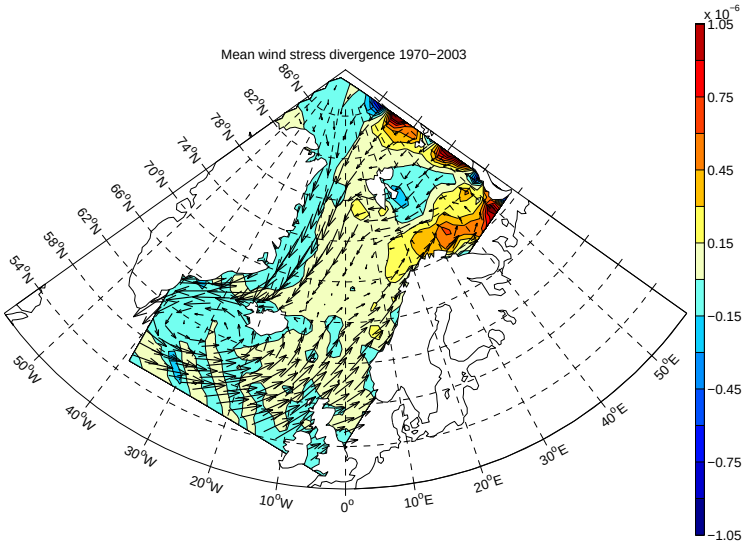

Figure 23: Mean wind stress divergence in N/m^3 1970–2003 (colours). Arrows as in Figure 21.

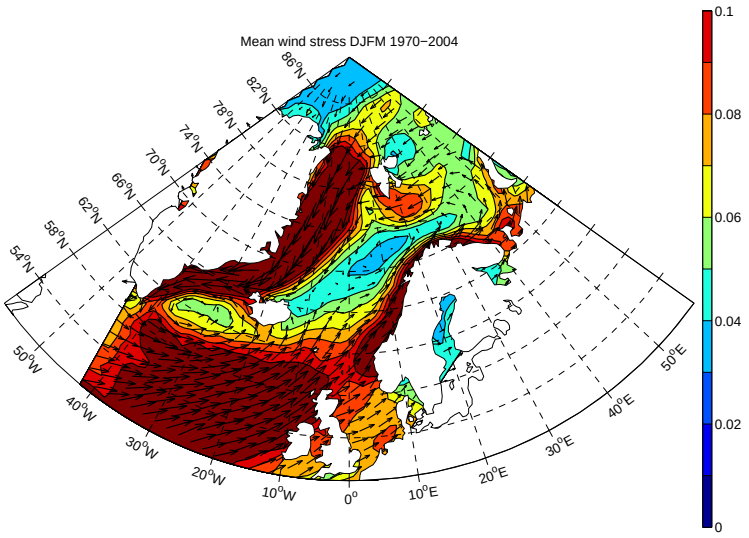

Figure 24: Mean wind stress in winter (DJFM) 1970–2004. Arrows indicate the direction and realtive strength of the wind stress, colours the wind stress magnitude in N/m^2.

Barents Sea, where negative wind stress prevails during summer, as can be seen in Figure 28. The high values for the wind stress divergence in the Barents Sea in the annual mean is not found during summer (Figure 29). Instead, there is a belt of negative wind stress divergence extending from the east of Svalbard to Novaya Zemlya.

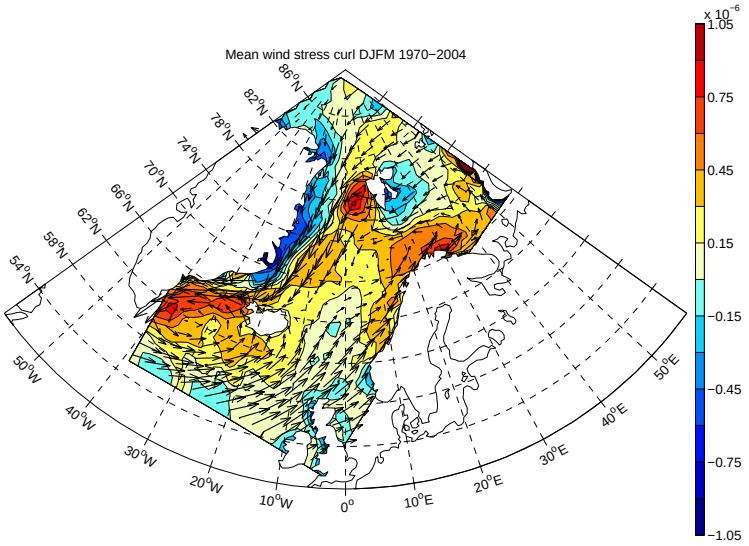

Figure 25: Mean wind stress curl in N/m^3 in winter (DJFM) 1970–2004 (colours). Arrows as in Figure 24.

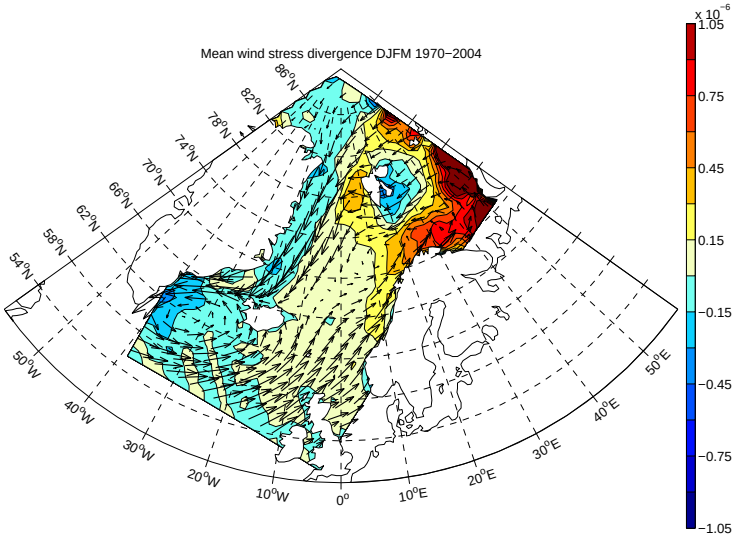

Figure 26: Mean wind stress divergence in N/m^3 in winter (DJFM) 1970–2004 (colours). Arrows as in Figure 24.

In the following, only winter will be considered, since the influence of the wind stress on the sea ice is expected to be stronger then. Furthermore, the sea ice covered area reaches far enough south, into areas where the wind stress data are more reliable.

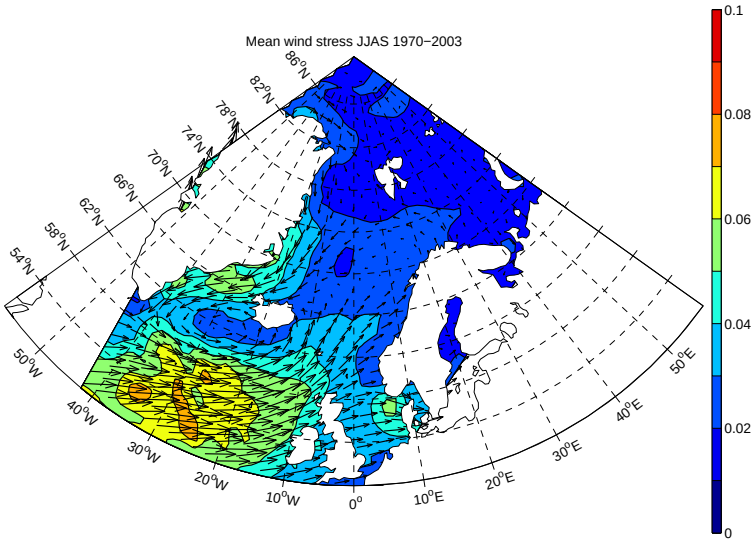

Figure 27: Mean wind stress in summer (JJAS) 1970–2003. Arrows indicate the direction and relative strength of the wind stress, colours the wind stress magnitude in N/m^2.

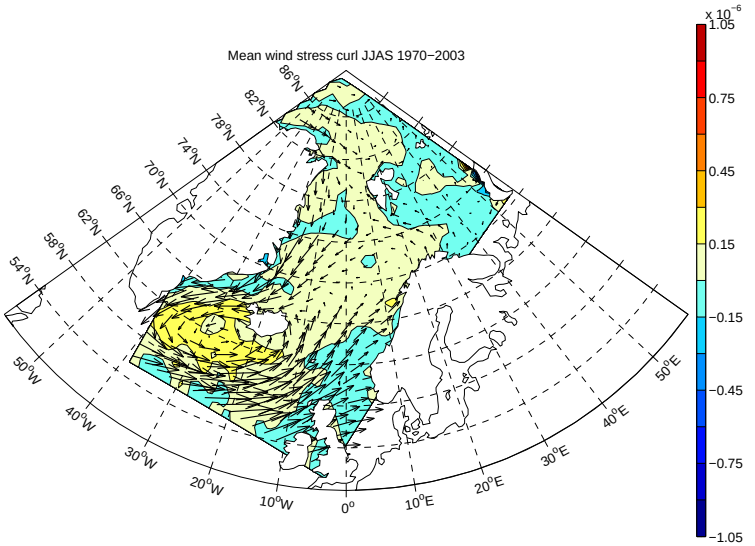

Figure 28: Mean wind stress curl in N/m^3 in summer (JJAS) 1970–2003 (colours). Arrows as in Figure 27.

3.1.3 Wind stress and the NAO

To get insight into how much the wind stress over the Nordic Seas is controlled by large scale-atmospheric circulations, it is compared with the winter (DJFM) NAO index (see Section 2.5). The Spearman Rank correlation (see

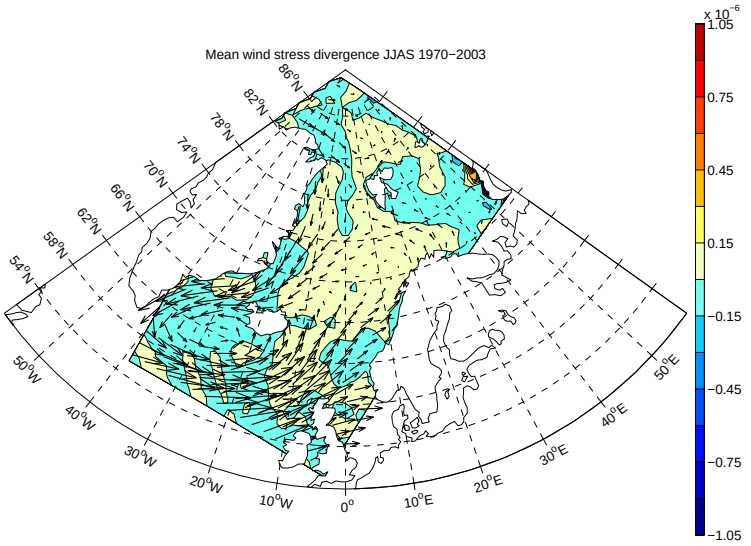

Figure 29: Mean wind stress divergence in N/m^3 in summer (JJAS) 1970–2003 (colours). Arrows as in Figure 27.

Section 2.2.2) between the DJFM mean of the eastward (τ_x) and northward (τ_y) components of the wind stress, the wind stress curl and the wind stress divergence and the winter NAO index is calculated at every grid point.

The DJFM mean of τ_x shows a significant negative correlation with the NAO in the northern Barents Sea, north of about 75^oN (see Figure 30). It is strongest in the area around Svalbard and over the Fram Strait up to the coast of Greenland. There is no significant correlation in the southern part of the Barents Sea, but a strong significant positive correlation can be found extending from the Norwegian coast to the south coast of Greenland. A significant positive correlation between the DJFM mean of τ_y and the NAO can be found in the southern and eastern Barents Sea, at some patches in the central Barents Sea and at the west coast of Svalbard (see Figure 31). The strongest negative correlations can be found along the east coast of Greenland, the strongest positive ones between Norway and the British Islands. For both τ_x and τ_y, the strongest correlations to the NAO are found outside the Barents Sea.

The wind stress curl shows significant positive correlations with the NAO index in the central Barents Sea and west of Svalbard extending in two belts southward through the Norwegian Sea to the area around Island (see Figure 32). Patches of significant negative correlation can be found south of Franz Josef Land, in the northern part of Storfjorden, at the east coast of Nordausland, along the coast of Norway and the east coast of Greenland. Figure 33 shows the correlations between the wind stress divergence and the

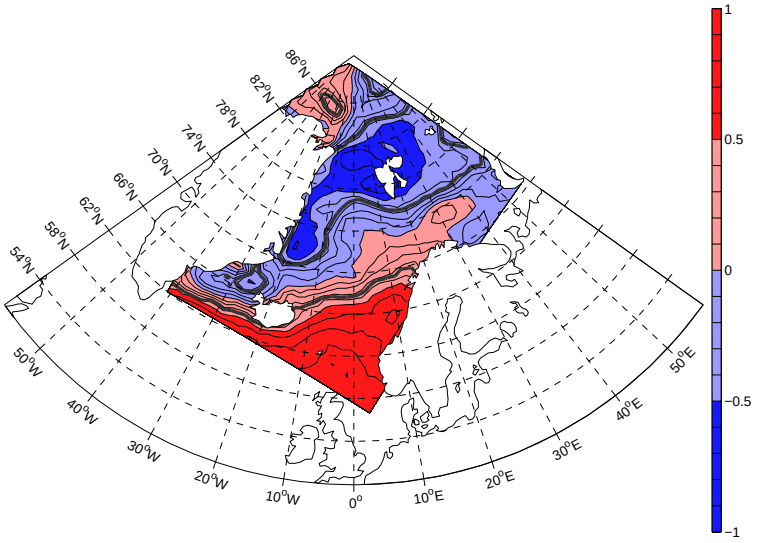

Figure 30: Map of Spearman Rank correlations between time series of the DJFM mean of τ_x and the NAO index 1970–2004. Red indicates positive, blue negative correlations. The 95% confidence level is shown by the thick grey line.

NAO index. Here patches of significant positive correlation can be found at several places in the centre of the Nordic Seas and in the central Barents Sea. Significant negative correlations can be found south of Franz Josef Land, in Storfjorden, in the northern part of the east coast of Greenland, at the west coast of Norway and west of Iceland.

Since NAO index and wind stress data are available before 1970, the same correlation maps were calculated for 1955–2004. The main difference to the results for 1970–2004 is that correlations in the Barents Sea are weaker and only small patches of significant correlations can be found there (not shown). A comparison between the wind stress fields and the Arctic Oscillation Index (AO) (from NOAA, http://www.cpc.ncep.noaa.gov/products/precip/CWlink/ENSO/verf/new.ao.shtml) leads to similar results as for the NAO (not shown).

3.2 The ice indices for the Barents Sea

The different ice indices used for the Barents Sea show in general a similar behaviour (see Figure 11). They are all significantly correlated with each other, the Spearman Rank correlation coefficient can be seen in Table 2. The correlation between I_w and the NAO is also significant, but not those of the two other ice indices with the NAO, when regarding the period 1970 - 2003. The correlation between I_{BKS} and the NAO becomes significant, when

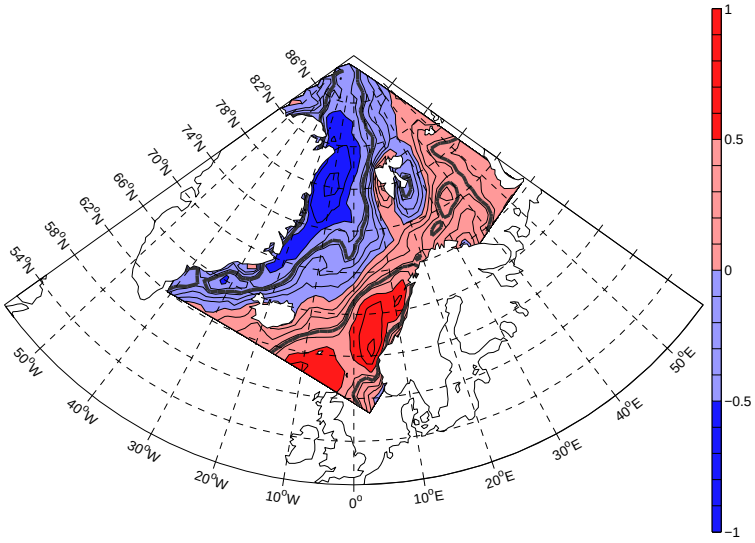

Figure 31: Map of Spearman Rank correlations between time series of the DJFM mean of τ_y and the NAO index 1970–2004. Colour convention as in Figure 30.

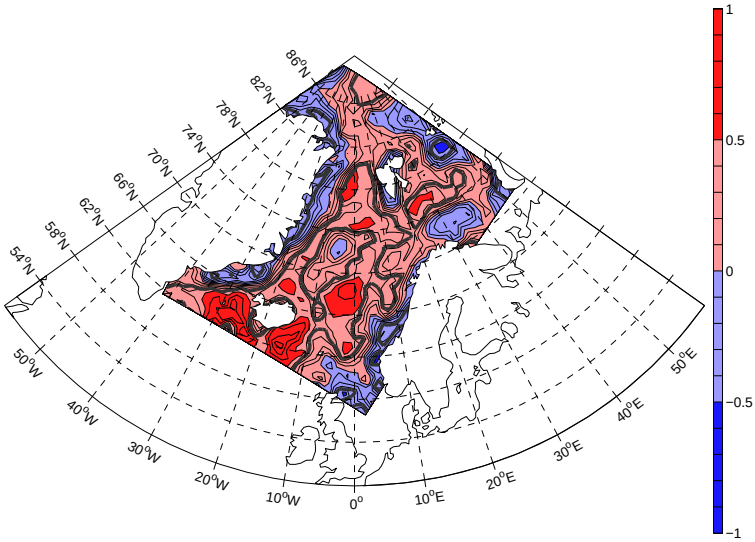

Figure 32: Map of Spearman Rank correlations between time series of the DJFM mean of the wind stress curl and the NAO index 1970–2004. Colour convention as in Figure 30.

the longest possible period is considered (1968–2004, $r_s = -0.40$, $p_s = 0.01$).

However, the ice indices show differences among each other and therefore, each of them is compared with the wind stress field to estimate the influence of the wind stress on the ice extent in the Barents Sea.

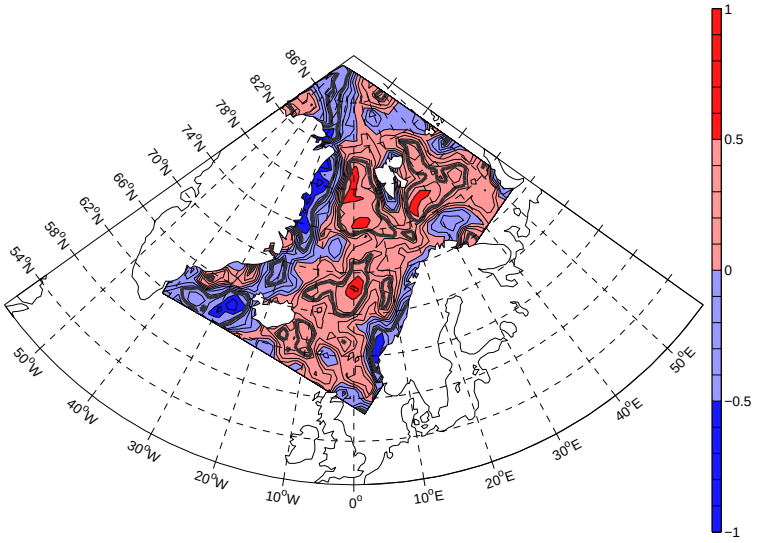

Figure 33: Map of Spearman Rank correlations between time series of the DJFM mean of the wind stress divergence and the NAO Index index 1970–2004. Colour convention as in Figure 30.

Table 2: Spearman Rank Correlation coefficient r_s between the different ice indices for the years 1970– 2003. Significant correlation ($p_s \leq 0.05$) are marked by bolt numbers.

Index	I_w	I_{BKB}	I_{BKS}	NAO
I_w	x	**0.79**	**0.71**	**-0.44**
I_{BKB}	**0.79**	x	**0.65**	-0.15
I_{BKS}	**0.71**	**0.65**	x	-0.33
NAO	**-0.44**	-0.15	-0.33	x

3.2.1 The Barents Sea Ice Index by Harald Loeng

To estimate the influence of the wind stress on the ice extent in the central Barents Sea, the Spearman Rank correlation between the winter (DJFM) means of the different wind stress variables and I_w is calculated at every grid point for the period from 1970 to 2003. The wind stress is strongest in DJFM, so that the strongest influence on the winter ice extent is expected in this period, although the maximum ice extent often occurs in April. The result is shown in Figure 34 for τ_x, in Figure 35 for τ_y, in Figure 36 for the wind stress curl and in Figure 37 for the wind stress divergence.

τ_x shows positive correlations with I_w larger than 0.5 north of 82^{o}N in the Arctic Ocean and significant negative correlations (but smaller than 0.5) in the central Barents Sea south of 74^{o}N (see Figure 34). τ_y has the largest cor-

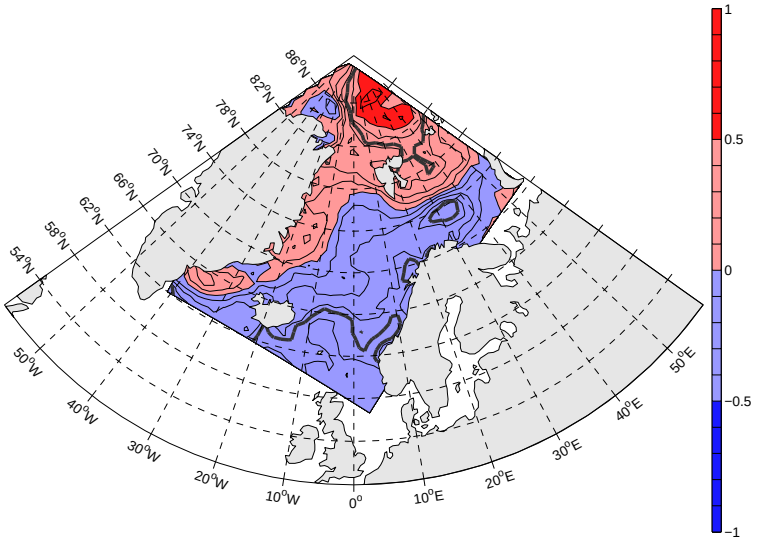

Figure 34: Map of Spearman Rank correlations between τ_x (DJFM mean) and I_w 1970–2003. Red indicates positive, blue negative correlations. The 95% confidence level is shown by the thick grey line.

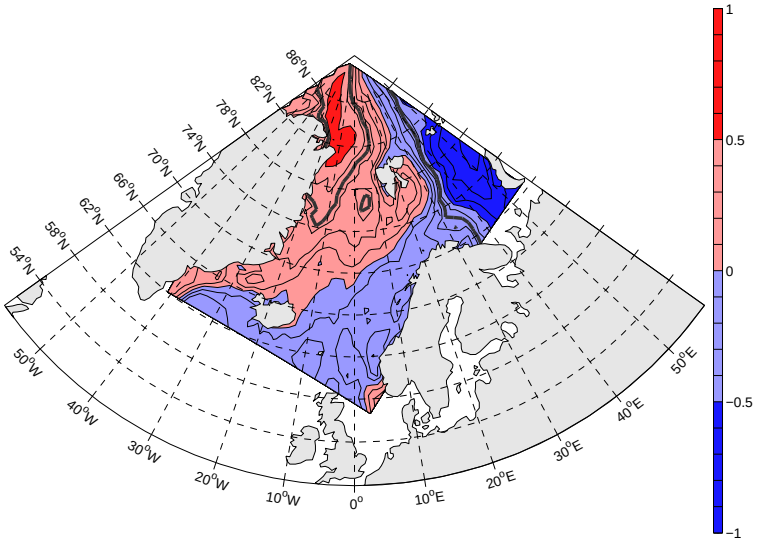

Figure 35: Map of Spearman Rank correlations between τ_y (DJFM mean) and I_w 1970–2003. Colour convention as in Figure 34.

relation with I_w of all wind stress variables. The largest negative correlations are located in the eastern Barents Sea, with values up to r=-0.88 at 76.3^{o}N, 35.0^{o}E (see Figure 35). A significant positive correlation can be found in the northeastern part of the Fram Strait.

For both the wind stress curl and the wind stress divergence strong neg-

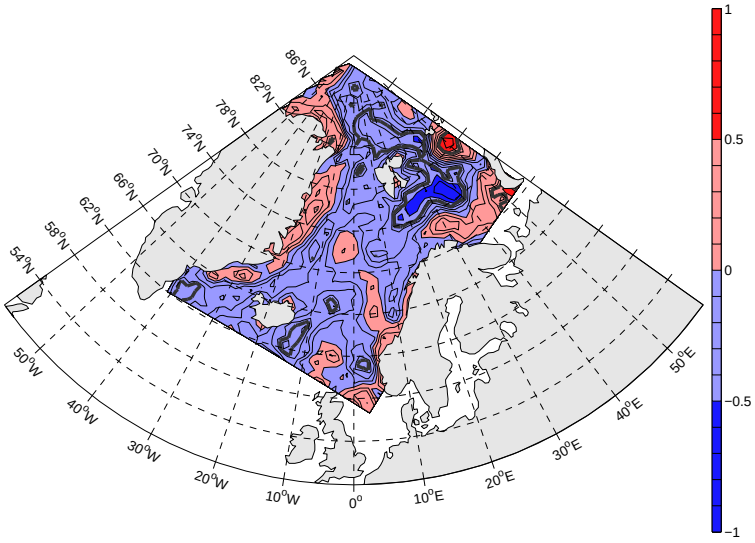

Figure 36: Map of Spearman Rank correlations between the wind stress curl (DJFM mean) and I_w 1970–2003. Colour convention as in Figure 34.

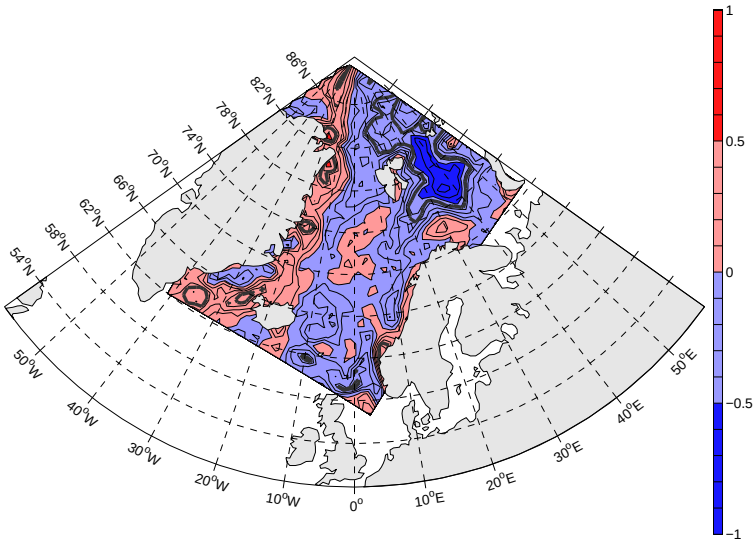

Figure 37: Map of Spearman Rank correlations between the of wind stress divergence (DJFM mean) and I_w 1970–2003. Colour convention as in Figure 34.

ative correlations with I_w can be found in the central Barents Sea at about 76^{o}N, the region of the winter ice edge. For the wind stress divergence, this region extents further to the north. An area with positive correlations above 0.5 between the wind stress curl and I_w can be seen at about 78^{o}N south of Franz Josef Land. There are also several small areas with significant

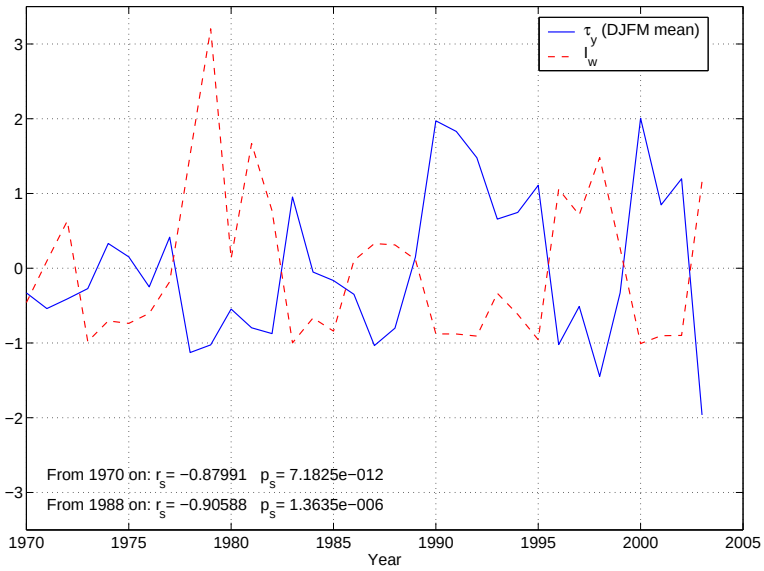

Figure 38: Time series of τ_y at 76.3^oN, 35.0^oE and I_w. Both series are normalized for comparison. The Spearman rank correlation coefficient(r_s) and its significance (p_s) are given for 1970–2003 and for 1988–2003.

correlations in the Norwegian and Greenland Sea.

The strongest negative correlation between τ_y and I_w are close to the coast of Novaya Zemlya, as mentioned above. The normalized time series at 76.3°N, 35.0°E are shown in Figure 38. The correlation is somewhat larger when only the years after 1987 are regarded ($r_s = -0.91$ compared to $r_s = -0.88$ for the whole time period). Figure 39 shows a scatter plot of I_w and τ_y. Three time periods are marked by different symbols because the wind stress data are based on pressure maps from different models in this periods, as explained in Section 2.3. The regression line is only calculated for the values starting in 1988. For these recent years the relationship between the northward component of the wind stress for DJFM and I_w is fairly linear, the regression has a mistake of about 9% in increase and 14% of the intersection. The correlation maps shown in Figures 34 to 37 were also calculated for the shorter time periods 1982–2003 and 1988–2003. In these cases the correlations get larger, but their patterns do not change substantially (not shown). Figure 38 shows, that there are no strong trends in the time series. I_w decreases about 1.1 %, while the mean meridional wind stress component increases with by 4.8 % from 1970 to 2003.

To get more insight in the connections between the wind stress and I_w Figure 40 shows the wind stress field for winters (DJFM) with low I_w ($I_w < \overline{I_w} - 0.5 \cdot std(I_w)$, where $\overline{I_w}$ is the average over time and $std(I_w)$ is the standard deviation of I_w) and high I_w ($I_w > \overline{I_w} + 0.5 \cdot std(I_w)$). Years with

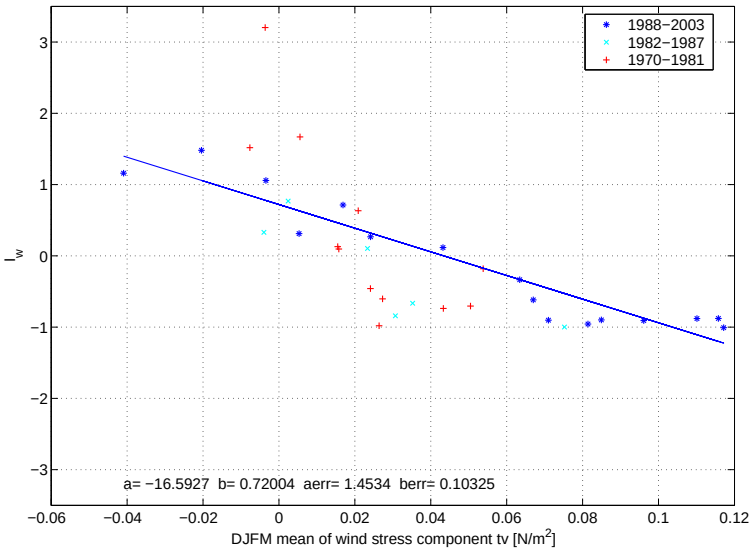

Figure 39: Scatter plot of τ_y in N/m^2 at 76.3^oN, 35.0^oE and I_w. Values from the period 1970-1981 are plotted as plus symbols, from 1982-1987 as crosses and starting in 1988 as stars.

a high I_w are: 1972, 1978, 1979, 1981, 1982, 1996–1998, 2003; years with a low I_w are: 1973–1976, 1983–1985, 1990–1992, 1994, 1995 and 2000–2002 (see Figure 11). The same comparison is also performed for the wind stress curl and the wind stress divergence in Figure 41 and 42, respectively.

Figure 40 shows that the cyclonic rotation of the wind stress field over the central Barents Sea is located more south and the southeasterly winds along the coast of Novaya Zemlya are weaker for years with high I_w. At the same time the northerly wind stress along the east coast of Greenland is weaker as well as the southwesterly wind stress south of Iceland and along the coast of Norway.

The main difference for the wind stress curl and divergence is that the area of negative values east of Svalbard is smaller in years with low I_w as can be seen in Figures 41 and 42. Additionally, the region of positive wind stress curl between Iceland and the Fram Strait and from there on to the coast of northern Norway is more intense in years with low I_w. Finally, the region of positive wind stress divergence in the eastern Barents Sea displays higher values.

3.2.2 The indices of ice extent by Børge Kvingedal

Index of ice extent for the whole Barents Sea I_{BKB}

The Spearman Rank correlation between I_{BKB} and the different parameters of the wind stress field (in DJF) can be seen in Figures 43 to 46. τ_x shows

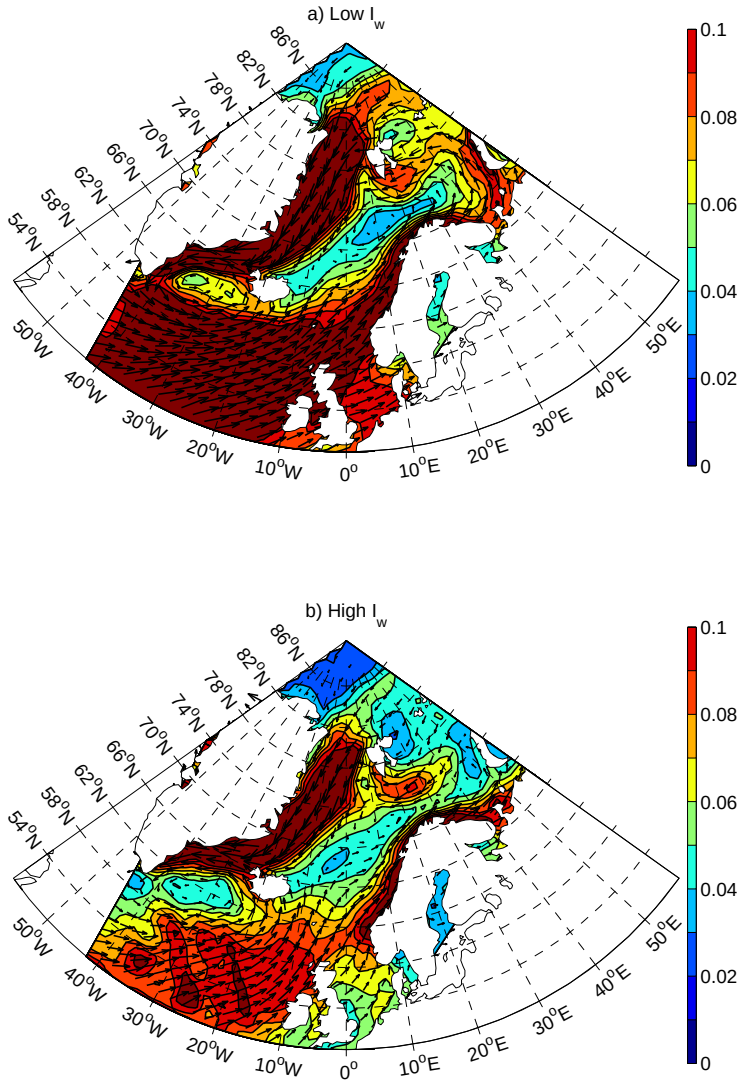

Figure 40: Mean wind stress for winters (DJFM) with a) low and b) high I_w. The arrows show the direction, colour the magnitude in N/m^2.

a significant negative correlation in the south and central Barents Sea, with a correlation coefficient up to $r_s = -0.4$ and a significant positive correlation (up to $r_s = 0.7$) north of Svalbard at about 86^oN. τ_y shows a significant negative correlation (up to $r_s = -0.7$) in the eastern Barents Sea and a significant positive one (up to $r_s = 0.5$) northeast of Greenland. Both these correlations are weaker and centred further in the north than for I_w (see Figures 34 and 35). The zero line between Greenland and Svalbard is further in the east compared to the I_w correlations. In general, the pattern of correlations between τ_x and τ_y and I_{BKB} are similar to those using I_w (see Figure 34).

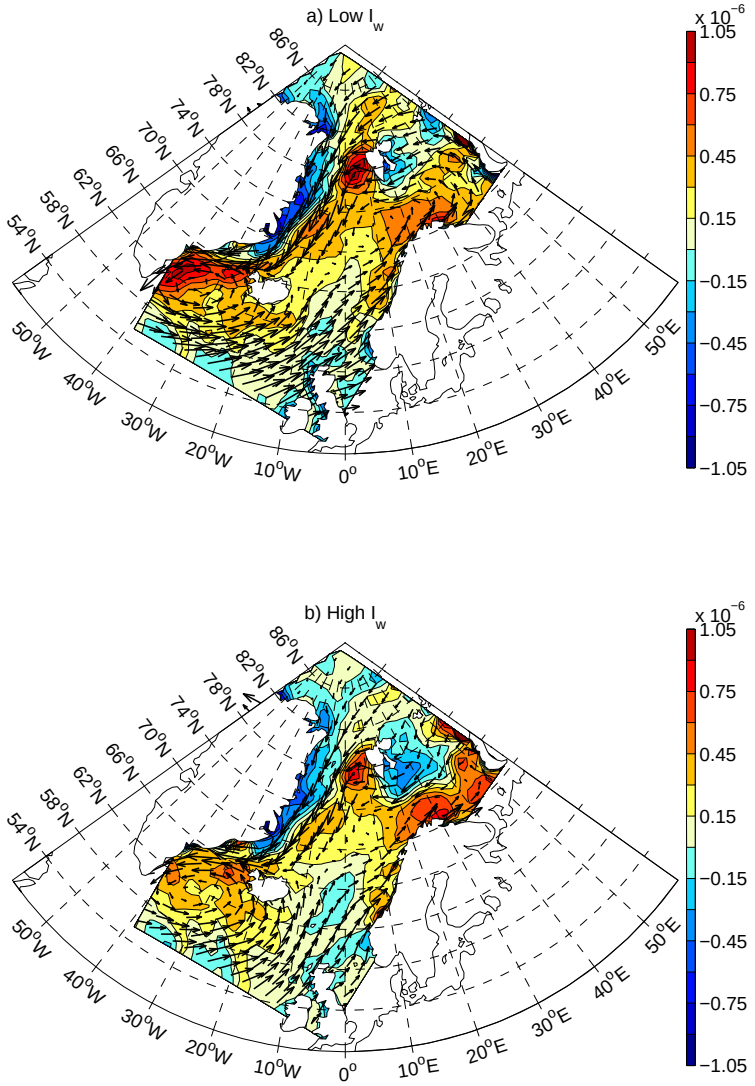

Figure 41: Mean wind stress curl in N/m^3 for winters (DJFM) with a) low and b) high I_w. Red indicates a positive blue a negative curl. Arrows as in Figure 40.

The wind stress curl is correlated significantly negative (up to $r_s = -0.4$) with I_{BKB} in several patches in the region where the ice edge can be found frequently and in a larger area north of Svalbard (up to $r_s = -0.5$). Significant positive correlations can be found south of Franz Josef Land (up to $r_s = 0.5$) and at the south coast of Novaya Zemlya (up to $r_s = 0.3$)(see Figure 45). The correlations, however are much lower than those using I_w (see Figure 36). For the wind stress divergence, the area of significant negative correlation to I_{BKB} east of Svalbard is about the same as with I_w (see

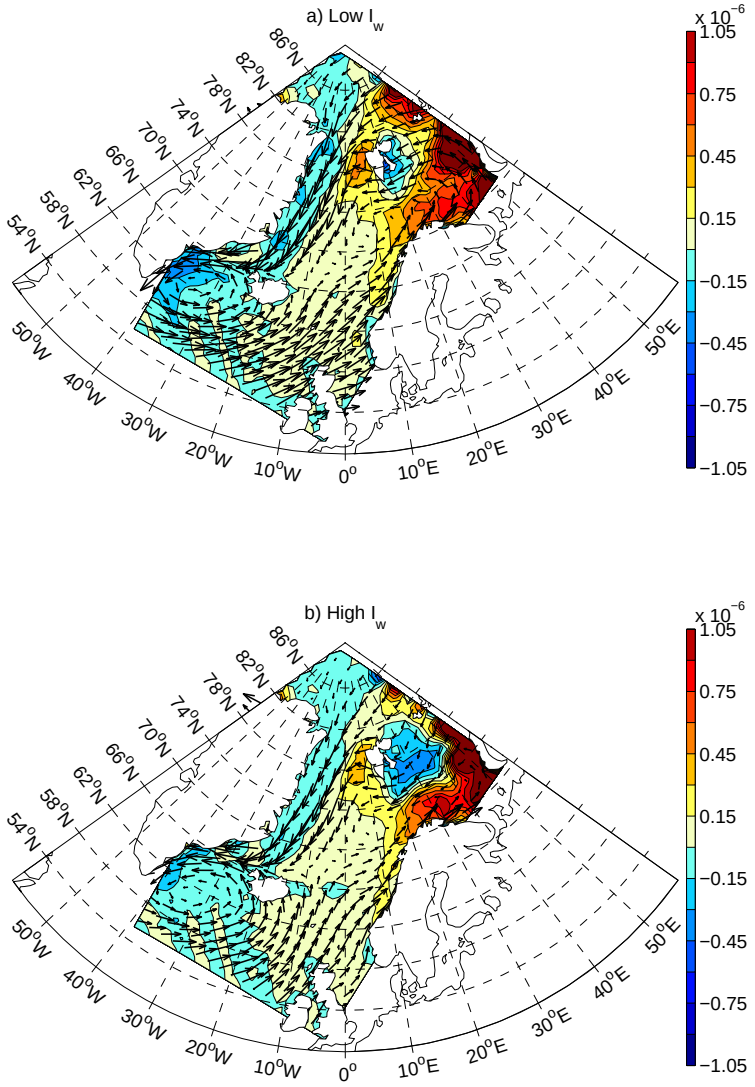

Figure 42: Mean wind stress divergence in N/m^3 for winters (DJFM) with a) low and b) high I_w. Red indicates a positive blue a negative divergence. Arrows as in Figure 40.

Figures 37 and 46), but the correlations are again weaker (up to $r_s = -0.5$ for I_{BKB} and up to $r_s = -0.7$ for I_w) and the strongest correlations are located somewhat further in the north as for I_w. As in the case of I_w, several small patches with significant correlations are found in the Norwegian and Greenland Seas.

The years with low I_{BKB} ($< 0.5std$): 1973–1975, 1984, 1985, 1990–1993, 2000–2002 and 2005. Apart from 1993 and 2005 these have also a low I_w. High I_{BKB} ($> 0.5std$) are observed in the years: 1967–1969, 1979–1982, 1988,

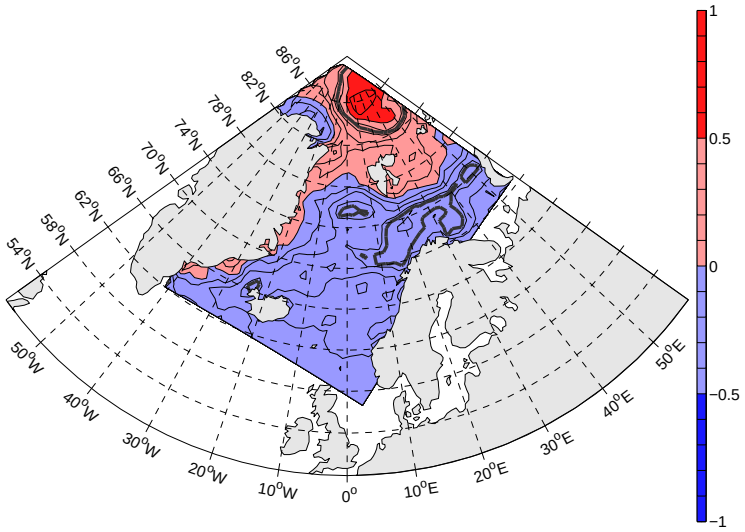

Figure 43: Map of Spearman Rank correlations between τ_x (DJF mean) and I_{BKB} 1970–2004. Red indicates positive, blue negative correlations. The 95% confidence level is limited by the thick grey line.

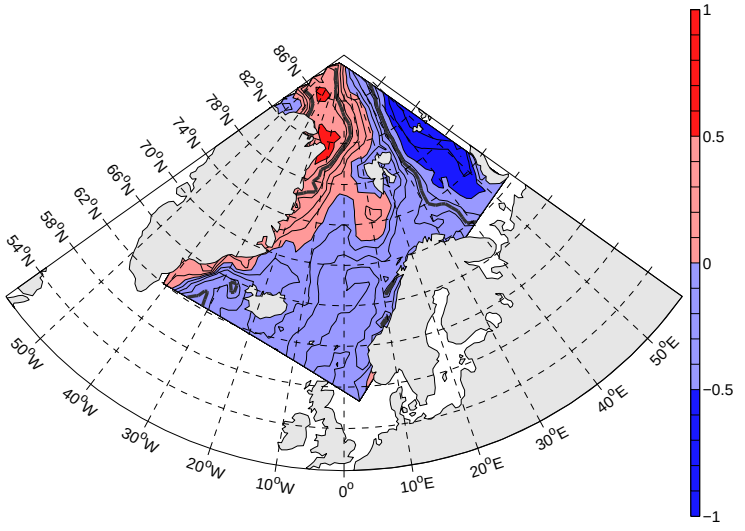

Figure 44: Map of Spearman Rank correlations between τ_y (DJF mean) and I_{BKB} 1970–2004). Colour convention as in Figure 43.

1989, 1996, 1998, 1999, 2003 and 2004 (see Figure 11). Six of these years have also a high I_w. Therefore the mean wind stress fields for years with low and high indices are about the same for I_{BKB} and I_w (not shown).

Index of ice extent south of Storfjorden I_{BKS}

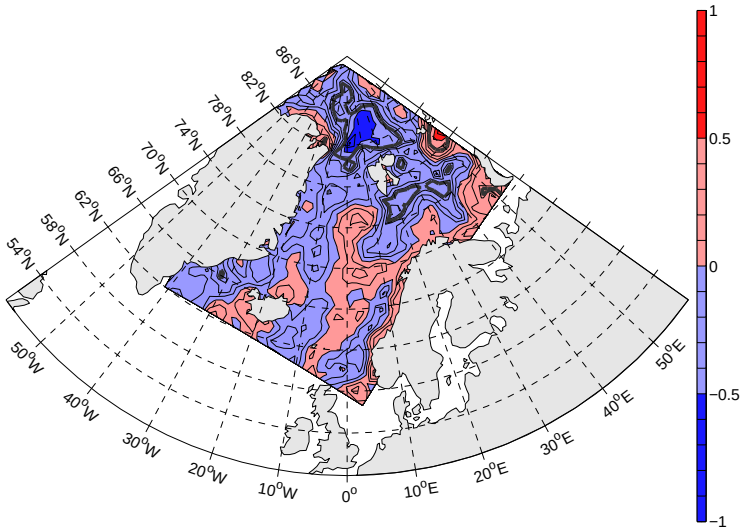

Figure 45: Map of Spearman Rank correlations betweenthe wind stress curl (DJF mean) and I_{BKB} (1970–2004). Colour convention as in Figure 43.

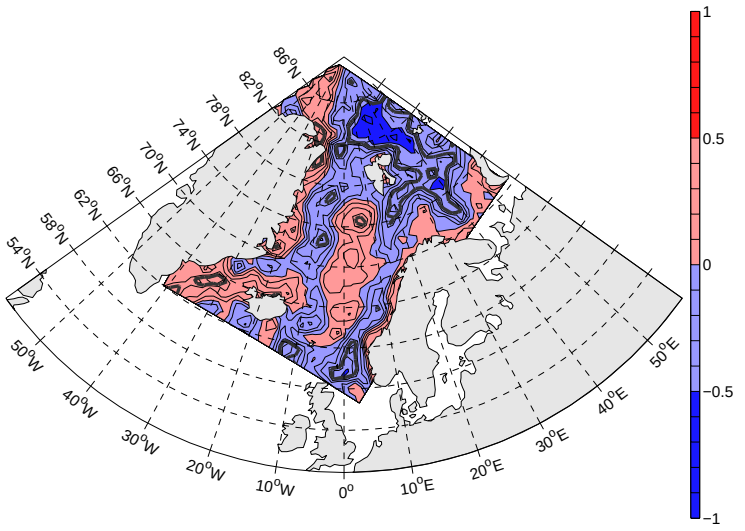

Figure 46: Map of Spearman Rank correlations between the wind stress divergence (DJF mean) and I_{BKB} (1970–2004). Colour convention as in Figure 43.

For the opening and closing of the polynya in Storfjorden, the ice extent in a region south of the fjord mouth is assumed to be most relevant, as explained in Section 2.4.4. Therefore an index of ice extent for the region south of 78^{o}N between 12^{o}E and 31^{o}E for the winters (DJFMA) 1968–2004 was defined by Børge Kvingedal (pers. comm.). Figures 47 to 50 show the

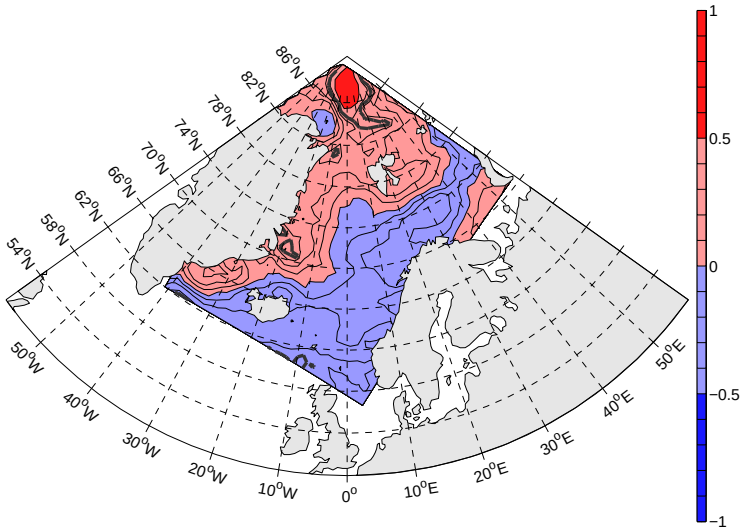

Figure 47: Map of Spearman Rank correlations between τ_x (DJFMA mean) and I_{BKS} 1970–2004. Red indicates positive, blue negative correlations. The 95% confidence level is limited by the thick grey line.

correlations of I_{BKS} with the different parameters of the wind stress field.

For τ_x the correlation patterns are similar to those with I_{BKB} (see Figure 47). The maximum of the significant negative correlation between τ_y and I_{BKS} is shifted into the central Barents Sea compared to those for I_w and I_{BKB} (Figure 48). The northward wind stress shows a significant negative correlation about everywhere east of Svalbard and the central Norwegian Sea. An exception is a spot exactly at Hopen Island, where the correlation is about zero.

Both the wind stress curl and the wind stress divergence show a patch with significant negative correlation to I_{BKS} south of Storfjorden (Figures 49 and 50). For the wind stress curl a positive correlation can be seen at the entrance of the Barents Sea, close to the north coast of Norway. This correlation is not significant for I_{BKS} in contrast to those using other two ice indices (Figures 36 and 45).

3.3 The polynya model for Storfjorden

The polynya model for Storfjorden needs two empirical factors as an input, the opening (OF) and the closing factor (CF) as described in Section 2.4.4. They were derived yearly and parameterize the ability of the polynya to open and to close. This ability is assumed to be influenced by the wind, the temperature and the ice conditions in Storfjorden and near the fjord mouth (Skogseth et al. 2004).

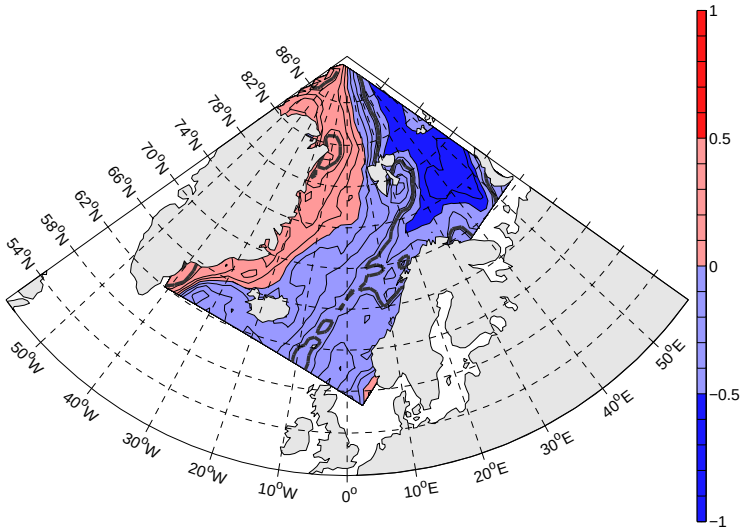

Figure 48: Map of Spearman Rank correlations between τ_y (DJFMA mean) and I_{BKS} 1970–2004. Colour convention as in Figure 47.

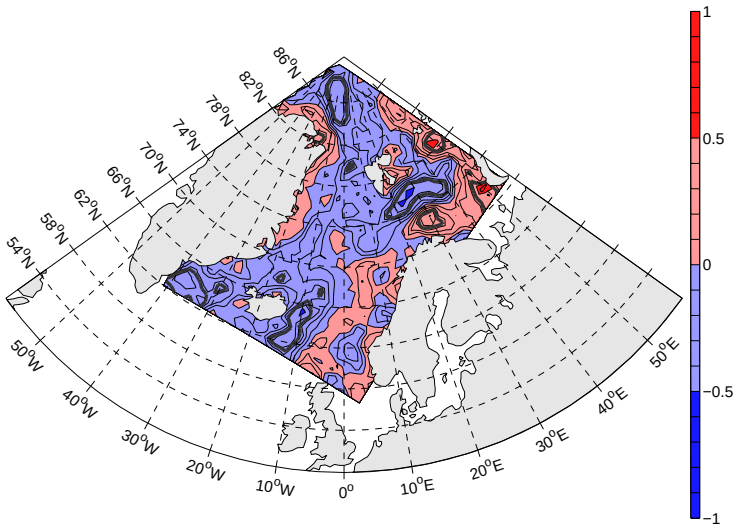

Figure 49: Map of Spearman Rank correlations between the wind stress curl (DJFMA mean) and I_{BKS} 1970–2004. Colour convention as in Figure 47.

For the winters 1998–2002 OF and CF are from Skogseth et al. (2004) and Skogseth (pers. comm.). They were derived for 2003 and 2004 by comparing the polynya width modelled with different OFs and CFs to satellite images (see Section 2.4.4). The best fit for these years can be seen in Figure 51. The different symbols describe the image quality (i.e. how well it was possible to destinguish water and thin ice areas from pack ice) and if the polynya was

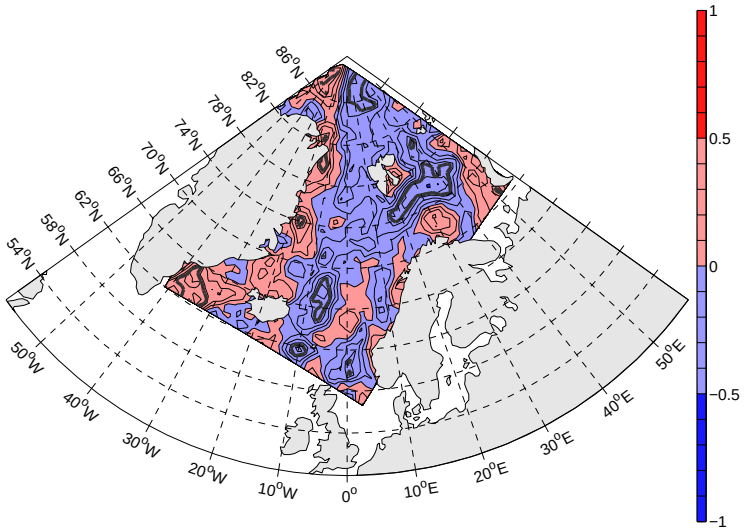

Figure 50: Map of Spearman Rank correlations between the wind stress divergence (DJFMA mean) and I_{BKS} 1970–2004. Colour convention as in Figure 47.

Table 3: Opening (OF) and closing (CF) factors for the polynya model.

Year	1998	1999	2000	2001	2002	2003	2004
OF	1	1.8	1	1.3	1.5	0.75	1.1
CF	15	13	20	19	15	7	20

opening from west instead of from north. The modelled polynya width was adjusted to fit best to the polynya width estimated from satellite images, giving images of good and average quality a higher weight. Openings from the west were ignored, because the model cannot cover them (because of $cos(\Phi_n - \Phi_0) \approx 0$). Table 3 shows OF snd CF for the winters 1998–2004.

Since these factors are assumed to be mainly dependent on the ice conditions outside Storfjorden, they are compared with the different wind stress parameters in this area, to investigate if similar connections between them and the wind stress can be found as between the ice indices and the wind stress. Figures 52 to 55 show the correlations between the winter mean (DJFMA) of different wind stress parameters and OF and CF. A standard (not a Spearman Rank) correlation is used, because the time series with 7 values are rather short.

There is a patch significant neative correlations between τ_x and OF right of Barentsnøya (Figure 52) and one of significant positive correlation for τ_x and OF in the central Barents Sea (Figure 53). No significant correlations

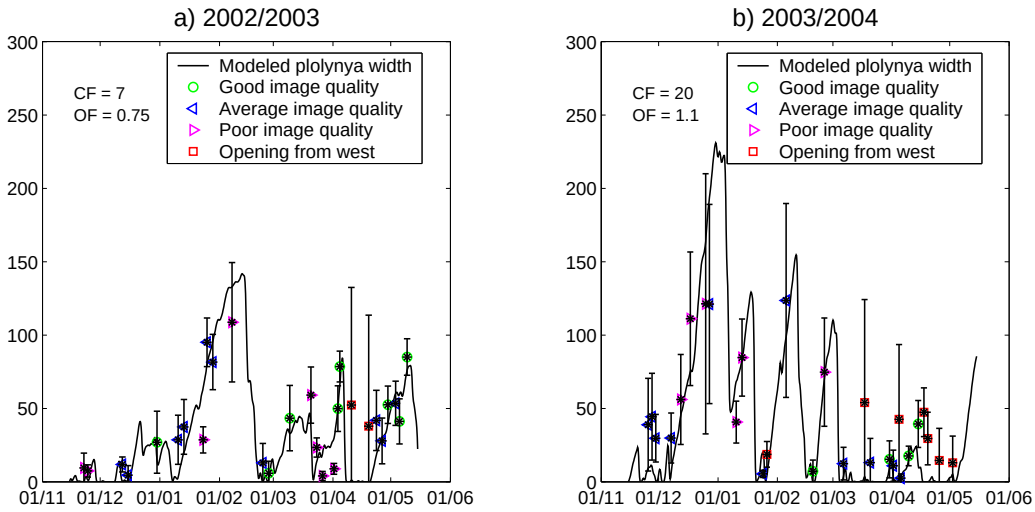

Figure 51: Best fit between the modelled polynya width and the one estimated from satellite images for a) 2002/2003 and b) 2003/2004. The different symbols display the quality of the satellite images or indicate if the polynya opened from west.

between τ_x or τ_y and CF can be found close to Svalbard. The highest correlation is found between the wind stress curl and OF, with r=0.97 in the Barents Sea, south of the fjord mouth of Storfjorden at about 75.4^{o}N, 25.1^{o}E, which is significant at the 95% level. The correlations between the wind stress divergence and OF and CF are similar to the ones for the wind stress curl but weaker (Figure 55).

Since it can be assumed that OF depends on the ice in front of the outlet of Storfjorden, Figure 56 shows scatter plots of the different ice indices and the wind stress curl at 75.4^{o}N, 25.1^{o}E together with OF. In the upper left panel, the scatter plot of the mean DJFMA wind stress curl (75.4^{o}N,25.1^{o}E) and OF can be seen. It shows the highest correlation (r=0.97) of all four panels. The correlation between I_{BKS} and OF is significant either (r=-0.77, p=0.04). The correlations of the other two ice indices are not significant (see upper right and lower left panel).

CF is significantly correlated to the wind stress curl north of Svalbard at 80.3^{o}N and 31.4^{o}E (Figure 54), but this correlation could not be explained physically. There are no other obvious connections between CF and the wind stress field (Figure 52 to 55). The comparison between CF and OF and the ice indices can be seen in Figure 57. Neigther OF nor one of the ice indices is significantly correlated to CF. The values for the winter 2002/2003 are marked with a red circle because of the unusual wide opening from west of the polynya that year (see Section 4).

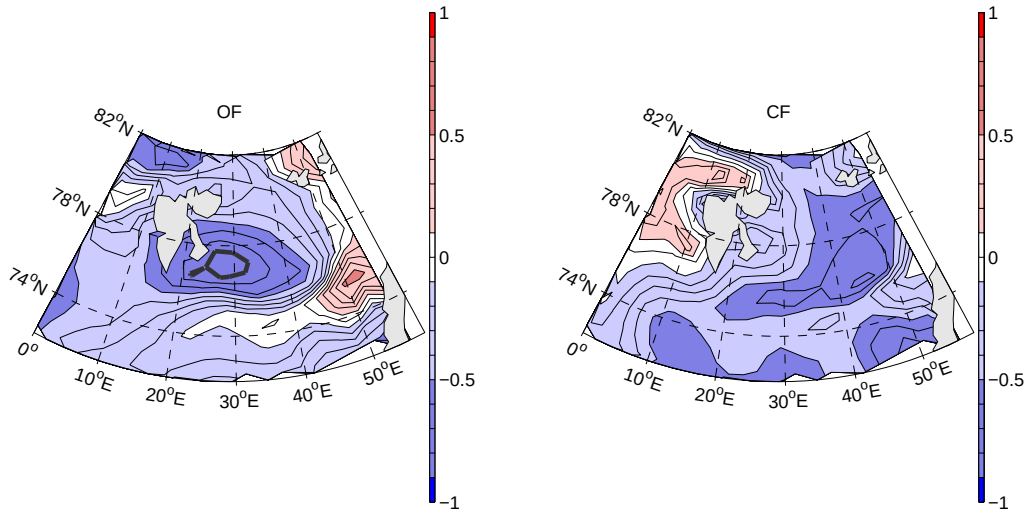

Figure 52: Map of correlations between τ_x and OF (left panel) and CF (right panel) 1998–2004. Red sindicates positive, blue negative correlations. The 95% confidence level is limited by the thick grey line. Correlations above ± 0.9 are displayed by dark colours.

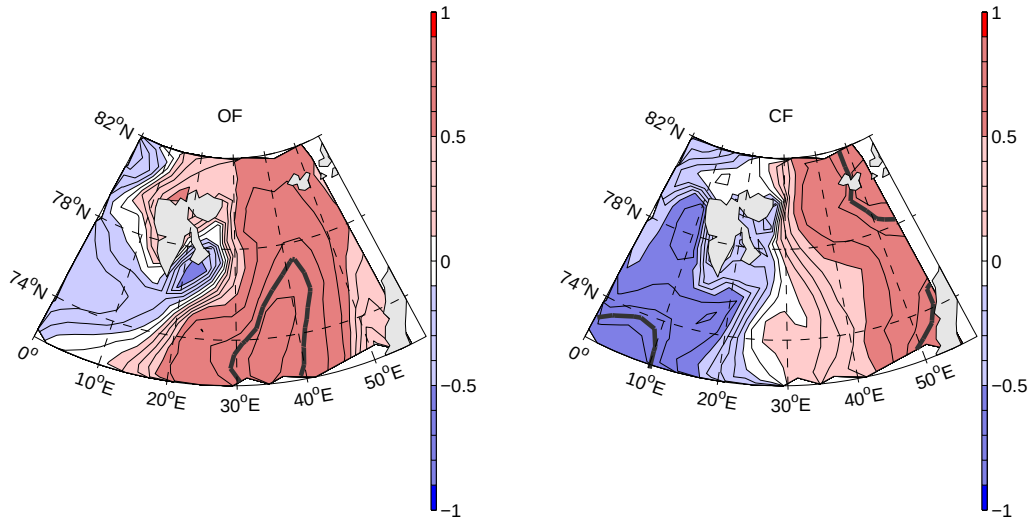

Figure 53: Map of correlations between τ_y and OF (left panel) and CF (right panel) 1998–2004. Colour convention as in Figure 52.

Due to the results from Figure 56, OF is estimated by a linear regression with a) the mean DJFMA wind stress curl at 75.4^{o}N, 25.1^{o}E ($OF = OF(\nabla \times \vec{\tau})$) and b) I_{BKS} ($OF = OF(I_{BKS})$) for the years 1970-2004 (Figure 58). CF is set constant to CF=19, as in Skogseth et al. (2005). OF($\nabla \times \vec{\tau}$) and OF(I_{BKS}) are in general similar, they are significantly correlated with

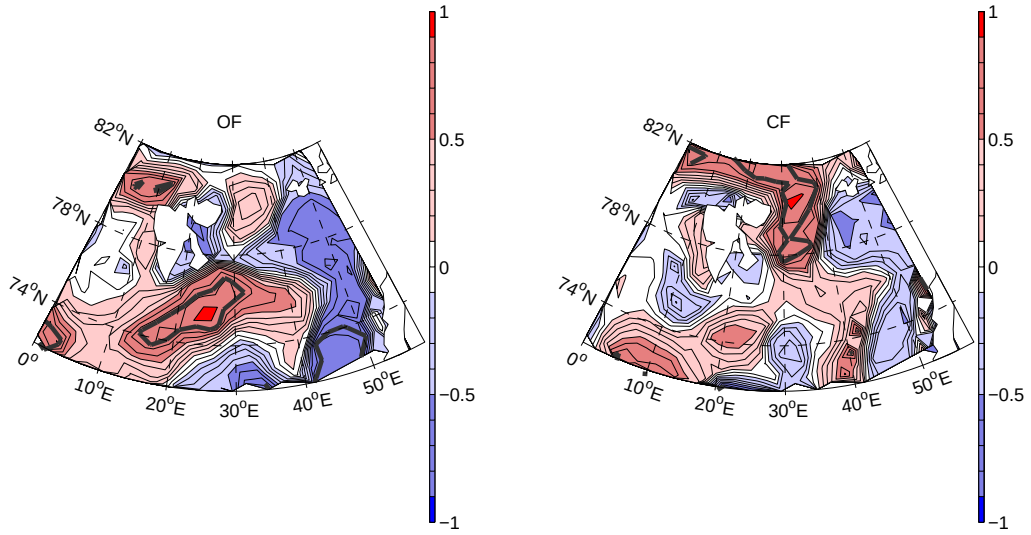

Figure 54: Map of correlations between time series of the wind stress curl and OF (left panel) and CF (right panel) 1998–2004. Colour convention as in Figure 52.

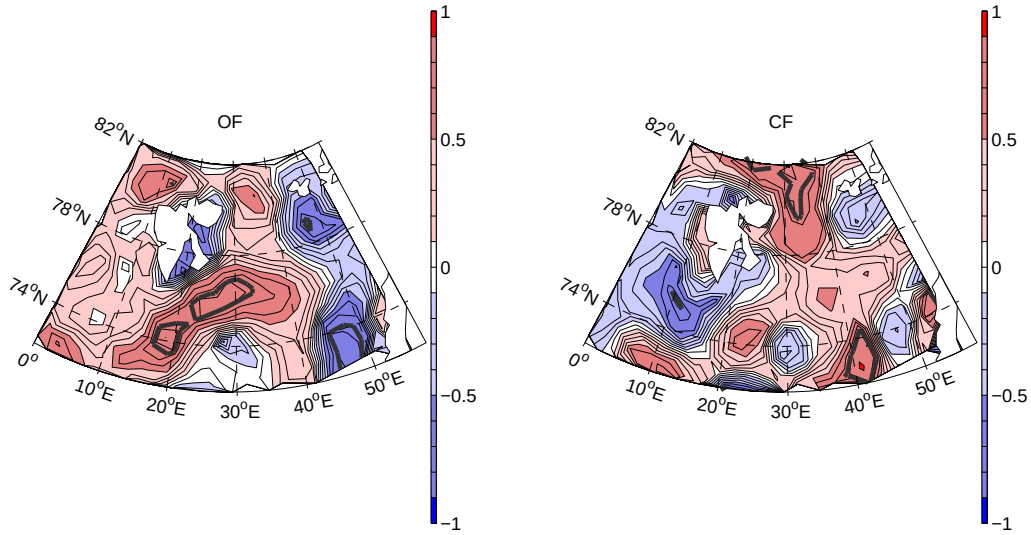

Figure 55: Map of correlations between time series of the wind stress divergence and OF (left panel) and CF (right panel) 1998–2004. Colour convention as in Figure 52.

a Spearman Rank correlation coefficient of $r_s = 0.49$. $OF(\nabla \times \vec{\tau})$ shows a better fit to the data derived from the satellite pictures. Before 1988, OF(I_{BKS}) is in most cases higher than OF($\nabla \times \vec{\tau}$).

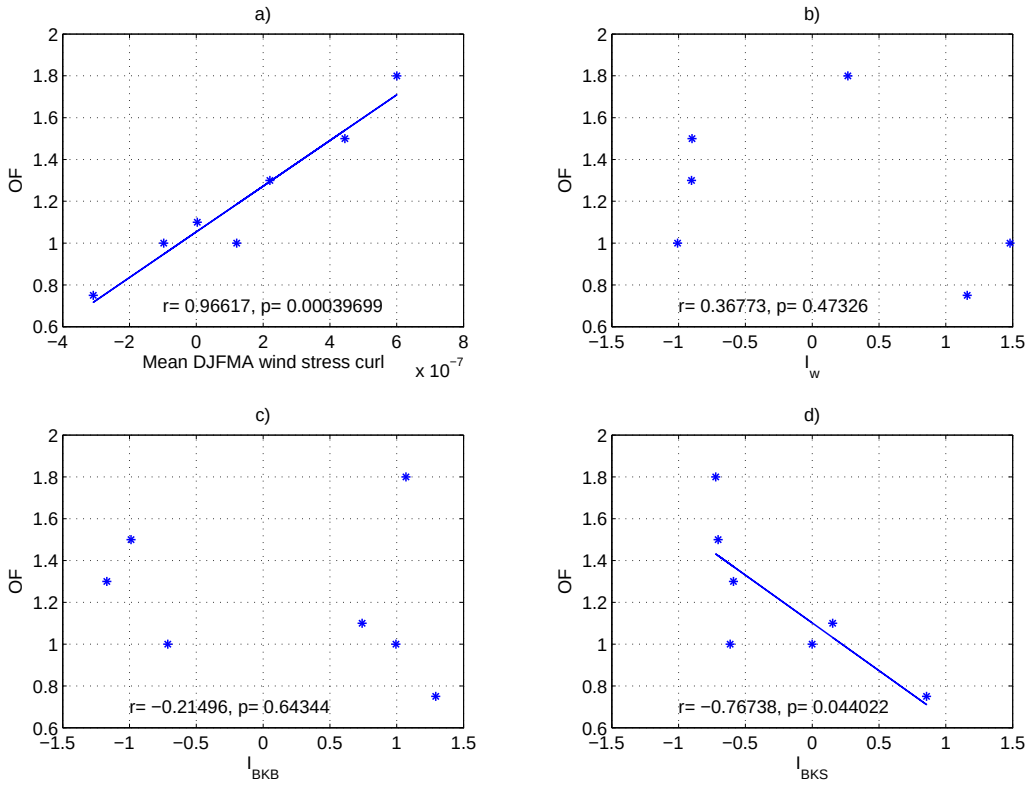

Figure 56: Scatter plot and regression lines of the mean OF with a) the mean DJFMA wind stress curl at 75.4^{o}N,25.1^{o}E (1998–2004), b) I_w (1998–2003), c) I_{BKB} (1998–2004), d) I_{BKS} (1998–2004).

These factors were now used as input parameters to the polynya model for Storfjorden. Figure 59 shows the total ice production (T_{is}) which results from model runs with different OF compared to maximum salinities measured in Storfjorden (see Section 2.6). The largest difference between the model runs are:

- In 1973 that with OF(I_{BKS}) shows a higher T_{is} than the others.
- In 1979 both OF(I_{BKS}) and $OF(\nabla \times \vec{\tau})$ lower T_{is} from a high to an average value.
- In 1986 to 1988 OF($\nabla \times \vec{\tau}$) leads to an increase of existing peaks and lowers T_{is} in 1987. The model run with OF(I_{BKS}) shows only one peak for T_{is} in 1986 and 1987 and a lower T_{is} than the other two model runs in 1988.
- In 1992 to 1995 T_{is} is increased by OF($\nabla \times \vec{\tau}$), especially in 1995 a remarkable peak appears.
- In 1996, 1997 and 2003 T_{is} is lowered compared to the run with constant OF when using OF($\nabla \times \vec{\tau}$) or OF(I_{BKS}).
- In 1999 to 2002 T_{is} is increased for OF($\nabla \times \vec{\tau}$) and OF(I_{BKS}).

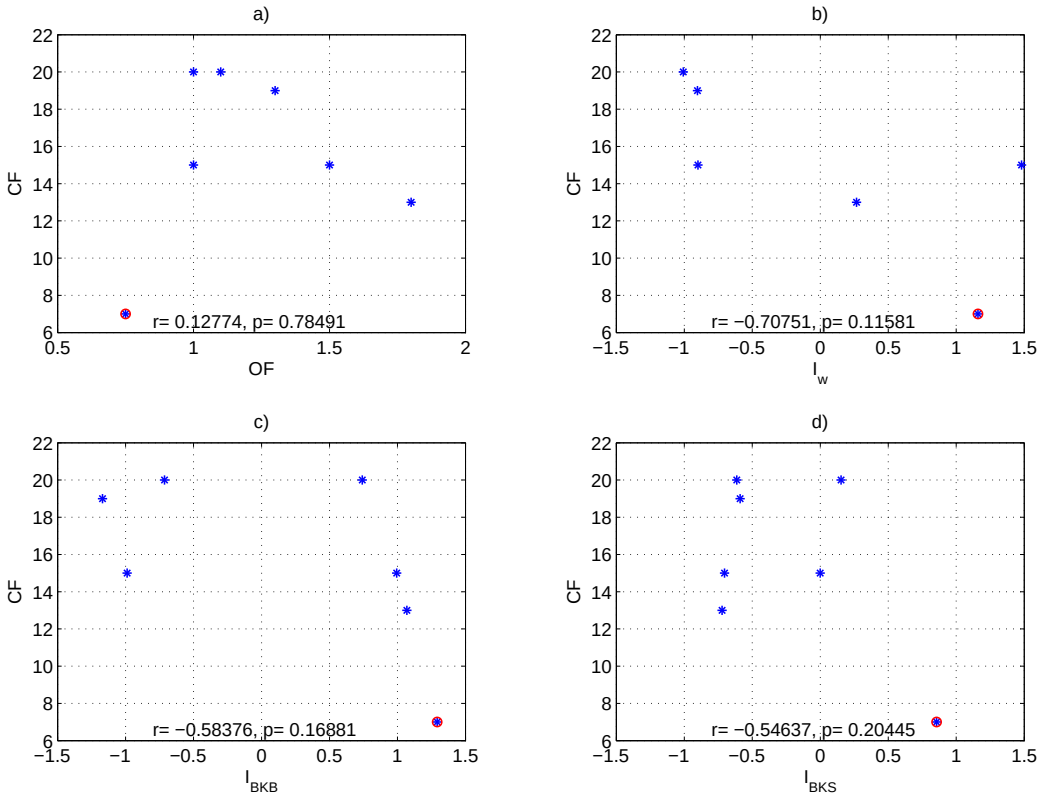

Figure 57: Scatter plot and regression lines of the mean CF with a) OF, b) I_w (1998–2003), c) I_{BKB} (1998–2004), d) I_{BKS} (1998–2004). The value for winter 2002/2003 is marked with a red circle.

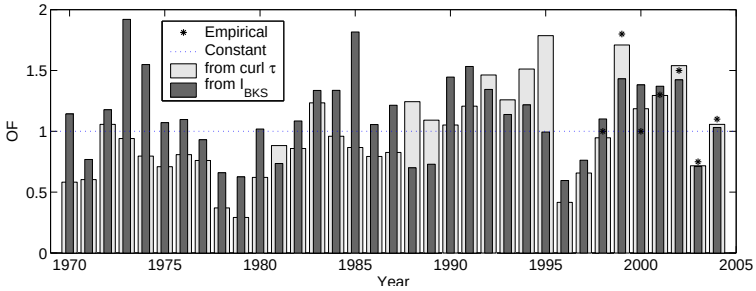

Figure 58: OF for the polynya model reproduced back to 1970. The light grey bars show $OF(\nabla \times \vec{\tau})$, the dark grey ones OF($I_{BKS}$). The stars show the values received by comparing the model output with satellite images and the dashed line shows the constant values used in Skogseth et al., (2004).

After 1998 a closer fit between the maximum salinities and the results from the model runs with variable OF can be seen. For earlier years it is difficult to make any statement. In 1984, 1985, 1989 and 1995 the salinities do not

agree with any of the model results. One should notice, that in 1989, 1994 and 1995 no BSW was found during autumn and summer (see Section 2.6).

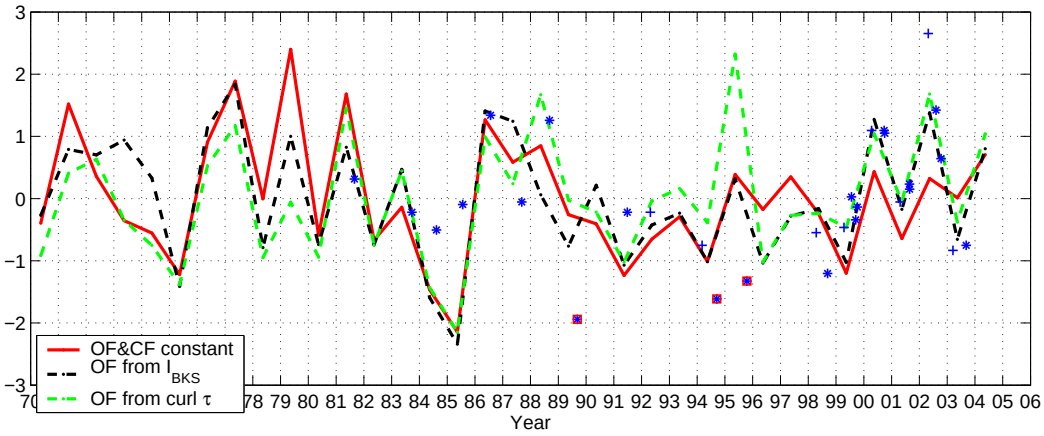

Figure 59: Red solid line: T_{is} from a model run with constant OF and CF. Black dashed line: T_{is} from a model run with OF($\nabla \times \vec{\tau}$) and CF=19. Green dashed line: T_{is} from a model run with OF(I_{BKS}) and CF=19. The stars show values of maximum salinity in Storfjorden measured between June and November, the crosses show those measured between January and May. Red squares indicate that no BSW was found. All values are normalized.

4 Discussion

4.1 The wind stress field over the Barents Sea

The comparison between the pressure field and the different wind stress parameters on 11 January 2001 (Figures 17 to 20) reveals that high absolute wind stress and positive wind stress curl and divergence are connected to low pressure systems and their fronts. The comparison at other dates shows similar results (not shown). For the wind stress magnitude and the wind stress curl this was expected, since low pressure systems are known to be connected to stronger winds and a cyclonic rotation.

For the wind stress divergence the opposite must have been expected, a the wind field convergent in the centre of a low pressure system. An explanation for the observed divergence can be that this convergence occurs on a too small scale to be resolved by the data set used here and the divergence is a result of the movement of the low pressure system. If a low pressure system approaches two points from southwest (what is usually the case in the central and northern Barents Sea, see Serreze et al. 1993), the wind stress will be higher at the point further west, which means that the zonal component of the wind stress (τ_x) increases in wind direction, which leads to a divergence (similar as in Arbetter et al. 2004: Where a low pressure system moving into a region with katabatic winds leads to a divergence).

The mean wind stress over the Barents Sea in winter is characterised by a cyclonic circulation centred in the central or western Barents Sea (see Figure 24). This circulation can also be found in the annual mean. It belongs to the North Atlantic Trough extending from Island through the Norwegian Sea into the central Barents Sea. This trough also marks the position of the main strom track, which enters the Barents Sea (see Murray and Simonds 1996, Serreze 1995) Although the influence of the NAO is stronger outside the Barents Sea, some significant correlations between the wind stress and the NAO could be found in the Barents Sea (Figure 30 to 33). Especially the wind stress curl and divergence in the central Barents Sea are influenced by the NAO, while its influence is weaker in the eastern Barents Sea or delays need to be taken into account. Therefore it can be assumed that the NAO is connected to the cyclonic circulation in the central Barents Sea, so the way that a high NAO leads to a stronger circulation located further east. In contrary not such a large influence of the NAO can be seen in the eastern Barents Sea.

4.2 The ice indices for the Barents Sea

All ice indices used are derived from the same data, but represent different regions. They are in general similar, indicated by significant Spearman Rank correlations between r=0.65 and r=0.79 for the years 1970–2003 (see Table 2). However, they also display several differences: The Barents Sea Ice Index by Harald Loeng (I_w) considers a smaller area but a longer period of each year, which agrees better with the maximum ice extend compared to the index by Børge Kvingedal (I_{BKB}). On the other hand I_{BKB} covers the whole Barents Sea. The index for the ice extent south of Storfjorden (I_{BKS}) represents an area that can be assumed to be most relevant for opening and closing of the Storfjorden polynya.

The Barents Sea Ice Index by Harald Loeng (I_w)

The significant correlations found in Figures 34–37 indicate, that the wind stress has a considerable influence on the distribution of sea ice in the central Barents Sea on interanual time scales.

The largest correlation can be found between τ_y and I_w in the eastern Barents Sea (Figure 36). Figure 40 shows that the mean wind stress is southerly in this area, both for winters with low and high I_w, but it is weaker in the case of high I_w. Thus a stronger northward wind in this area prevents the transport of ice into the central Barents Sea, while weaker winds or more frequent northerly winds leads to more sea ice. The highest correlation is found east of the area where I_w is defined. This agrees with the Nansen-Ekman drift law which states that the ice drifts with an angle of about 30^o to the right of the surface wind (see Section 2.1). It also agrees well with Furnes (1992), who used the same hindcast data set and found out that the ice extent in the Barents Sea increases under a northeasterly and decreases under a southeasterly wind regime. Not only the ice drift caused by the wind stress but also the advection of warm air from the south and with this enhanced melting or less freezing can influence the ice extent in connection with τ_y in the eastern Barents Sea.

The connection shown by the positive correlation northeast of Greenland (Figure 36) has no such strait forward explanation. A reason could be coherences within the wind field itself. In Figure 40, one can see that the northerly wind above northeast of Greenland is increased in years with low I_w compared to ones with high I_w. This can also link the ice conditions in the Barents Sea to those in the Fram Strait. Hilmer and Jung (2000) and Martin and Martin, Variability of Arctic Sea Ice Transports, submitted to Journal of Geophysical Research, (2004) found an increased ice transport through the Fram Strait contemporanous to an anomalous low surface pressure in the Barents Sea, which can be connected to a smaller ice extent (Vinje 2001).

Also Rogers et al. (2005) found less cyclones in the Barents Sea, when the ice export in the Fram Strait is high. Increased northerly winds northeast of Greenland will probably lead to a higher ice transport through the Fram Strait which gives rise to an anticorrelation between the Fram Strait and the Barents Sea. But for this correlation, one should also mention that it lays in an area with low data quality before 1987 (see Figure 8) and even though being significant, it does not necessarily reflects a real connection. For τ_x, no such clear connection to I_w is found. The highest correlation is situated north of Svalbard (Figure 34) in a region where the data quality is questionable (see Figure 7). One possible explanation it is that eastward wind stress in this area would lead to an ice transport to the southeast into the region east of Svalbard, so that a high amount of ice would be available there for a transport into the central Barents Sea. Similar to the positive correlation between τ_y and I_w, this also provides a possible link to the ice transport in the Fram Strait. A westward wind in this region would probably increase the amount of ice available for transport through the Fram Strait. There is also significant negative correlations between I_w and τ_x in the central Barents Sea, which is probably due to the change in the cyclonic circulation over the Barents Sea: It is weaker and centred further in the south in years with a high I_w. Therefore the stronger easterly wind stress (from north of the cyclonic circulation) can be found further in the south (see Figure 40) leading to a negative correlation in this area.

The negative correlation between I_w and the wind stress curl and divergence in the central Barents Sea is found at about 75.8^{o}N, 34.0^{o}E, approximately in the region of the ice edge in winter (e.g. Kvingedal and Sorteberg, submitted manusrcipt, 2005). The wind stress curl and divergence in this area are positive, when the cyclonic circulation usually found over the Barents Sea during winter reaches far north and is stronger. This leads to a southeasterly wind stress and prevents ice transport from the north east into this region (see Figures 40 to 42). At the same time more low pressure systems can come further north (a positive curl and divergence is often connected to low pressure systems see Figures 17, 19 and 20). This cyclonic circulation determents the position of the trough reaching from Iceland into the Barents Sea, as mentioned in Section 4.1. Low pressure systems are often connected to the advection of warm temperatures and to high wind speeds, which break the ice (Kvingedal and Sorteberg, submitted manuscript, 2005, Holt and Martin 2001). Additionally, less ice cover is connected to increased heat fluxes (Deser et al. 2000), which may indicate more or stronger low pressure systems. However, the model of Murray and Simmonds (1995) did not confirm this for the Arctic Ocean. Due to the relatively low heat fluxes and frequently occurring inversions over sea ice the corresponding wind stress is observed to be weaker over ice than over open water (Guest et al. 1995).

This decline in the wind speed leads to a divergence over the ice. A cyclonic circulation reaching far into the central Barents Sea is also connected to strong southerly winds in the eastern Barents Sea and therefore also reduces the ice extent as explained when regarding τ_y.

In the southern Barents Sea, a higher positive wind stress curl can be seen in years with high I_w (Figure 41). A reason may be that the low pressure systems are possibly stronger in this region in years with far south reaching sea ice. The presence of the ice edge increases the temperature gradient and therefore also the heat fluxes relative compared to years when the ice edge is located further north (Deser et al. 2000). The positive correlation between the wind stress curl and I_w in the eastern Barents sea south of Franz Josef Land north of the mean ice edge at about 78.4^{o}N, 50.9^{o}E indicates a change from positive wind stress curl in years with high I_w to negative curl in years with low I_w (Figure 41). The reason might be that low pressure systems, which are not entering the central Barents Sea during years with much ice follow the coast of Norway and Russia. From there they might move north along Novaya Zemlya. However, that this correlation occurs in an area where the data quality is questionable (see Figure 9).

This significant positive correlation between the wind stress curl and I_w south of Franz Josef Land and the positive one between the both, the wind stress curl and the wind stress divergence and I_w in the central Barents Sea are also found when comparing the wind stress curl and divergence to the NAO, but with opposite sign (see Figures 32 and 33). This indicates that the NAO influences the ice conditions in the Barents Sea through its influence on the wind stress field. A high NAO is connected to a stronger and further east located cyclonic circulation in the Barents Sea. However, the correlations of the NAO index and the different ice indices are not always significant (see Table 2) and weaker than those between the ice indices and the wind stress in certain areas. In particular, interannual fluctuations of τ_y in the east of the Barents Sea, which seems to be most important for the ice conditions (see Figures 35 and 44), can be not totally explained by the NAO (the correlation is significant but much lower than for the ice indices (see Figure 31)). This means, that also the local wind field or a delay in the dependency of the NAO is important.

Ingvaldson et al. (2004) discusses the influence of the wind stress on the inflow of Atlantic Water into the Barents Sea. Their wind field associated with increased inflow into the Barents Sea (their Figure 12) agrees well with the wind stress field found here that reduces the ice extent (Figure 40). This indicates that also the inflow of warm water and with it the position of the Arctic Front can have an influence on the sea ice extent. At the same time it makes it difficult to distinguish between the influence from the atmosphere and from the ocean.

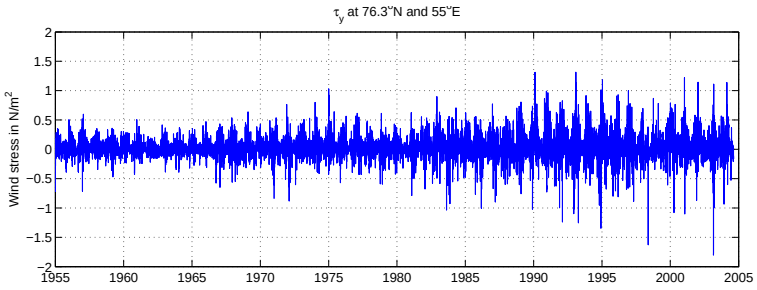

Figure 60: Time series of τ_y, at the point where the correlation of the DJFM mean of τ_y and I_w is strongest (at 76.3^oN, 35.0^oE).

In the scatter plot the relationship between the I_w and the DJFM mean of τ_y (Figure 39) seems to be not linear when regarding the whole time period. Considering only the years from 1988 it turns out to be fairly linear. A regression line is computed, and its error in slope is smaller than 10% for this period. One reason that this relationship is not found for the whole time period could be a negative trend in the ice extent which was found by several authors in the Barents Sea (e.g. Vinje and Kvambekk 1991, Maslanik et al. 1996, Kvingedal, submitted manuscript, 2005). The trend found in I_w however, amounds to -1.1% over 34, which years rather weak. Over the same time, τ_y increased by 4.8%, at the point where the correlation to I_w is strongest. This increase is probably artificial and caused by the lower data quality before 1982. As can be seen in Figure 60, τ_y shows smaller variations before 1982. The difference is not as big as further to the northwest (see Figure 6), but can nevertheless be assumed to have influenced the winter mean of the wind stress. This inhomogenity in the data quality makes it impossible to estimate if the trend in the ice extent is connected to changes in the mean wind field or caused by other factors like an increase in air temperature.

The Index of Barents Sea ice extent by Børge Kvingedal I_{BKB}

The pattern of correlations to τ_y are similar for I_{BKB} as for I_w, but the correlations are weaker and shifted further to the north (see Figure 44). This is probably caused by the index covering fewer month (DJF) and a larger region (see Figure 12 and 13). In particular the wider east-west extent of the area may weaken the correlation, because the influence of the wind stress differs over this large distance. The shift of the areas of strong correlation towards the north is probably related to the meridionally unbounded. For τ_x, the significant positive correlation with I_{BKB} is about the same as for I_w, while the area of the significant negative correlation in the Barents Sea has increased (Figure 43). The reason for this can be, that now a longer fraction

of the ice edge is included and so the wind stress in a larger area important for the extent.

For the wind stress curl and divergence the patches correlated to I_{BKB} are smaller and the magnitude of the correlations are smaller in the Barents Sea. A larger area makes the ice extent less dependent on the wind stress in one specific region. Furthermore, the path of the storm track can lead to a decrease of ice extent in one part and at the same time to an increase in another part. Therefore it is more promising to estimate the amount of ice in a smaller area with the wind stress curl and wind stress divergence. The smaller correlations between the wind stress curl and divergence and I_{BKB} in the central Barents Sea are consistent with the weaker (compared to I_w), not significant correlation between I_{BKB} and the NAO (see Table 2), since both NAO and I_w show higher correlations to the wind stress curl and divergence in this area. This supports as well the assumption that the NAO mainly influences the strength and position of the cyclonic circulation in the central Barents Sea and is less important in the eastern Barents Sea, because I_{BKB} represents a much larger area in the east than I_w (see Figures 12 and 13).

Both the wind stress curl and the wind stress divergence show a significant negative correlation north of Svalbard. The explanation may be again the connection of I_w to the ice transport through the Fram Strait mentioned already when discussing I_w, which could be increased when more low pressure systems move into this area. On the other data quality in this region is poor.

The index of the ice extent south of Storfjorden by Børge Kvingedal I_{BKS}

Here the significant negative correlations with the wind stress curl and the divergence are also found, in the region of ice edge in the area relevant for I_{BKS} (Figure 49 and 50). This shows that the variations in wind stress curl and divergence can be a measure for the position of the ice edge, if the area is not too large.

The connection between the northward wind stress component and the index is also valid in this case (Figure 48). The area where the largest correlations between I_{BKS} and τ_y are is located further to the west compared to the other two ice indices. This was expected, since also the area I_{BKS} is defined over lays westwards of those for I_w and I_{BKS}. At Hopen Island, no correlation between τ_y and I_{BKS} is found. The boundary at 78^oN may have been chosen too far northward. Therefore northerly winds, which increase the ice extent, would at the same time open the polynya, which reduces the ice extent from the north. Thus I_{BKS} does not increase during phases of strong northerly winds, because of the polynya. No ice can be transported there from north, because Heleysundet and Freemansundet, the sounds opening

Storfjorden to the northeast are often blocked by fast ice and are too narrow to allow the transport of ice into the fjord.

Comparing the indices

Comparing Figures 34–37 for I_w with the corresponding Figures 43–46 for I_{BKB}, gives the impression that the influence of the wind field on the ice in the central Barents Sea (represented by I_w) is much more pronounced than its influence on the ice cover of the whole Barents Sea. The area regarded by Børge Kvingedal is so large that different parts of it are influenced by different factors that may not exibit the same interannual variations. Additinolly delays can be important. Nevertheless the indices are similar, despite the fact that I_w just covers about 1/3 of the area of I_{BKB}. This fraction of the Barents Sea regarded for I_w shows the highest fluctuations in ice extent both seasonally and interannually (I_w covers an area between 25 and 45^{o}E, the area of highest variability of ice extent in the Barents Sea according to Sharpiro et al. (2001) between 25 and 49^{o}E). The influence of the ocean currents described for I_w may be similar either. I_{BKS} is similar to the other ice indices although it is covering a much smaller area. Especially the pattern of correlation are about the same appart from changing their location: The highest correlation in the Barents Sea exists again with τ_y followed by the wind stress curl and the wind stress divergence.

Altogether one can say that the wind stress plays an important role for the interannual changes in ice extent in the Barents Sea, especially its northward component in the east but also the wind stress curl and divergence in the central Barents Sea. They appear all to be connected to the location and intensity of the cyclonic circulation in the central Barents Sea. This findings agree well with Vinje and Kvambekk (2001), who stated that the position of the Barents Sea Low is especially important for the sea ice formation.

4.3 The polynya model for Storfjorden

The empirical opening (OF) and closing (CF) factors in the polynya model for Storfjorden were compared to the different ice indices and wind stress parameters. The highest correlations for OF was found with the wind stress curl at 75.4^{o}N, 25.1^{o}E (Figure 54). Of all ice indices, I_{BKS} shows, the highest correlation (Figure 56). This was expected, because I_{BKS} represents the area most relevant for the ice transport into and out of Storfjorden. The positive correlation between the wind stress curl and OF means that a reduced wind stress curl coincides with a lower OF. A negative or low wind stress curl indicates the passage of fewer low pressure systems and of a rather anticyclonic circulation. Under these conditions, the amount of ice in this area is

relatively high, as shown for the ice indices. Hence OF is low when there is a lot of ice in front of the opening of Storfjorden, blocking the outward transport of the ice in the fjord and therefore slowing down the opening of the polynya. Additionally, a negative wind stress curl and divergence lead to a convergent ice movement (see Section 2.1) and therefore increases the compactness of the ice cover. This increases the internal stress and slows the ice drift (Richter-Menge et al. 2002). The negative correlation between I_{BKS} and OF confirms these relations. The correlation here is lower in magnitude than that with the curl, because the area chosen is not ideal to be relevant for the polynya opening. OF is reproduced for both I_{BKS} and the wind stress curl at 75.4^{o}N, 25.1^{o}E for all years back to 1970.

No clear connection between CF and the wind stress or any of the ice indices could be found. Therefore it is kept constant with CF=19, which was also used in Skogseth et al. (2004). A connection between OF and CF could be expected, because when the polynya opens easyly (and therefore relatively wide) it will take more time to close it and sometimes little is ice available for closing. But no such connection was found. Reasons can be that a higher number of cyclones south of Storfjorden can break up the ice and allowing it to move faster (Brümmer et al. 2003), both into and out of the polynya and therefore also increase CF. Additionally, CF is also depends on other factors than the ice drift. Especially the frazil ice production, which is governed by the air temperature is probably more important (Skogseth et al. (2004)), but no clear connection to the temperature at Hopen Island could be found (not shown). One reason might be that high temperatures lead to a not so fast closing due to decreased freezing, but at the same time the speed of the ice drift can be increased due to looser bounds and less stresses between the flows, leading to a faster closing. An other possible connection might be that more cyclones in the Barents Sea (and therefore less ice) are connected to relativly cold temperatures on Svalbard (Rogers et al. 2005). Also the especially wide opening of the polynya from west in winter 2002/2003 can have an influence. An opening from the west was also observed in 2003/2004, but in the winter 2002/2003 the open water area was extremely large, as can be seen in Figure 61. Therefore nearly no ice was available to close the polynya afterwards. This is one possible explenation for the very low CF in 2002/2003 compared to all other years.

Figure 58 shows the reproduced OFs. OF($\nabla \times \vec{\tau}$) shows a closer fit to the empirical values than OF(I_{BKS}), as can be expected due to the higher correlation. Suspicious is that before 1988, the values for OF($\nabla \times \vec{\tau}$) are in general lower than those for OF(I_{BKS}). The reason therefore is probably a lower mean wind stress before 1988 which may be caused by the reduced quality of the wind stress data (see Section 2.3).

These reproduced OFs were used as input parameters to the polynya

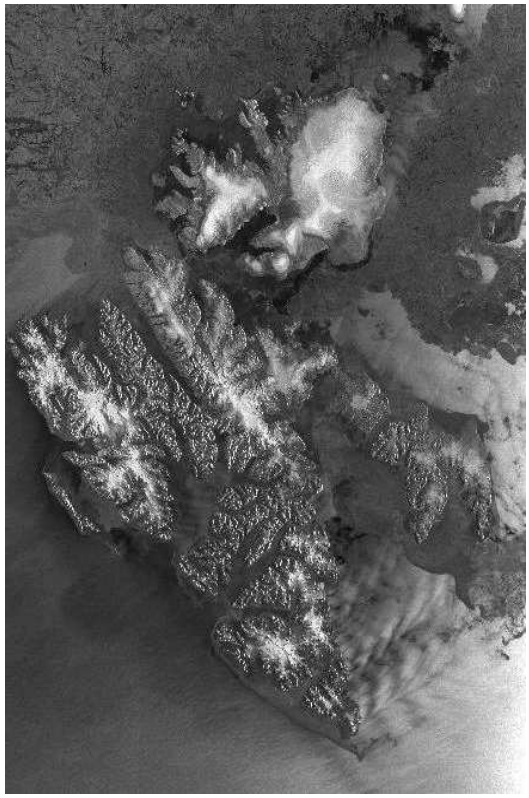

Figure 61: Envisat ASAR Quicklook image of the Storfjorden area from the EOLI Catalogue (http://muis-env.esrin.esa.it:8080/servlets/template/welcome/entryPage2.vm) from 19 April 2003. A large area of open water caused by strong westerly winds can be seen in the southern part of Storfjorden.

model. In addition the model was run with the constant OF and CF as in Skogseth et al. (2004), now including the winters 2002, 2003 and 2004. The resulting total ice productions (T_{is}) are compared to each other and to the maximum salinity measured in Storfjorden (see Figure 59). Including variable OF does change T_{is} in several years but theses changes follow no clear system. Using OF($\nabla \times \vec{\tau}$) and OF(I_{BKS}) leads to nearly identical T_{is} from 2000 onwards. Also the results for the 1990s are similar or this variable input parameters, appart from the large peak in 1995, which appears only for OF($\nabla \times \vec{\tau}$). Earlier the differences of T_{is} are about the same between all three model runs.

There are no salinities to compare with before 1981 and until 1998 not every year measurements where taken. In three years no BSW was fond although measurements where taken (see Section 2.6). Their salinities do not fit to any of the model runs (Figure 59). The measurement with relatively

low salinity in autumn 1995 disagrees with the large peak in ice production in 1995. It coincidents with a water temperature as high as $T = -1.5^{o}$C. In 1994 and 1989, the salinity is lower than 34.8 psu. It can be assumed, that possibly produced BSW had already left Storfjorden due to outflow and diffusion when this three measurements were taken and they are most likely not reflecting the BSW production of the previous winter and spring. This is supported by the fact that all this measurements are taken relatively late in the autumn, during September or October. Generally the outflow from Storfjorden poses an uncertainty for the comparison of T_{is} with the production of BSW. In the year 2002, were three salinity measurements are available (from 27 April, 7 August and 13 October) and the salinity decreased obviously during the summer, see Figure 59. Schauer (1995) found no BSW outflow from Storfjorden between October and December 1992 and assumed therefore that all BSW produced in the previous freezing season left out earlier. Hence it would be better to have salinity measure salinities at about the same time for each year, preferably in late May or June. Unfortunately, measurements in Storfjorden are just taken sporadically. Additionally, Storfjorden is often not accessible by boat before July due to the sea ice. In years with severe ice conditions like in winter 2003/2004 Storfjorden is still ice covered in July.

The model runs with variable OF show a better fit to the salinities than the model with constant OF and CF from 1999 onwards. Before 1999 it is hard to say if any of the model runs has advantages. The largest "improvements" happened in the time period when the salinity measurements are most exact and most frequent but also when OF was derived empirically. This means, that the wind stress curl and I_{BKS} proved to be useful to reproduce the (empirically derived) OF for recent years, but it is not possible to say something about the quality of the reproduction back in time, since there are to few measurements available to compare to.

That no reproduction of CF was possible, is probably because CF is influenced by several parameters. Although CF was set constant, the variable OF seems to have improved the modelled T_{is} for recent years. Therefore it would be interesting to estimate how big the influence of OF and CF on the model are. To do this, the model was run with constant CF=19 for both OF=0.75 and OF=1.8, the minimum and maximum empirical value for OF. The same was done with constant OF=1 and CF set to its minimum and maximum observed value, CF=7 and CF=20, respectively. The results are shown in Figure 62. It shows that a higher OF and a lower CF leads to more ice production compared to a lower OF and higher CF, as could be expected. The differences between T_{is} the minimum and maximum OF are larger than the ones for minmum and maximum CF for every year. The mean difference between the maximum and minimum for OF is $19.7km^3$ and for CF $7.1km^3$. This indicate, that OF has a larger influence on the model

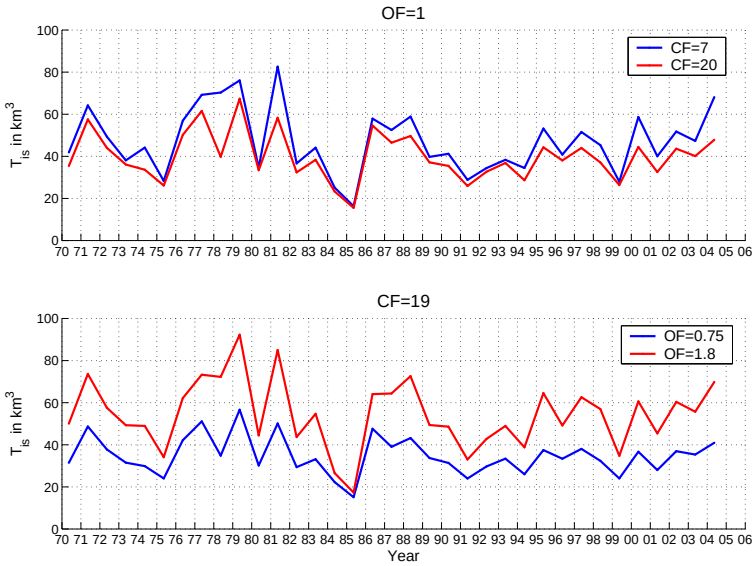

Figure 62: Upper panel: T_{is} for OF=1 and CF=20(red line) and CF=20(blue line). Lower panel: T_{is} for CF=19 and OF=1.8(red line) and OF=0.75(blue line)

result. The reason is most probably that the wind is more often blowing from northerly directions in the region of Storfjorden during winter. This is shown in Figure 63 which displays a histogram of wind directions for DJFMA of the years 1970-2004. It shows clearly that the wind is preferably northerly, so that there are much more cases when OF is applied.

Another possibility to compare T_{is} of the model with constant factors to that with variable ones is to reproduce the correlation to the NAO and I_w found in Skogseth et al. (2004). They found a significant positive Spearman Rank correlation between T_{is} and the Barents Sea Winter Ice Index (I_w) was found and a negative one between T_{is} and the NAO. Both correlations were largest when the two year running mean was compared (T_{is} - I_w: $r_s = 0.79$, T_{is} - NAO: $r_s = -0.53$ for the two year running mean). For T_{is} modelled with OF($\nabla \times \vec{\tau}$), this comparison is shown in Figure 64 and for T_{is} resulting from OF(I_{BKS}) in Figure 65. In addition to I_w also the other ice indices are shown in the upper panel of both figures. Their two year running means are rather similar (as expected due to the correlations shown in Table 2). They show a good agreement to T_{is} in most years before 1995, but after this year the relationship changes totally, so that there is no significant correlation. The main difference between T_{is} modelled with OF(I_{BKS}) and with OF($\nabla \times \vec{\tau}$) is that the peaks around 1981 and in the early 1990s do not exist for the one from OF(I_{BKS}). T_{is} from OF(I_{BKS}) is also significantly correlated to the NAO with $r_s = -0.36$ and $p_s = 0.035$. This correlation, however is weaker

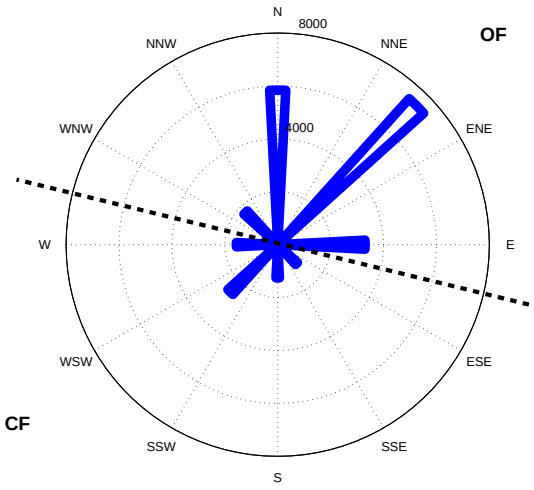

Figure 63: Rose plot of the histogram of the wind directions at Hopen Island during DJFMA 1970-2004. The dashed line marks for which wind direction OF and CF are used, respectivly. The numbers are the numbers of measurements for the wind directions

than that obtained by using constant factors. For I_w again no significant correlation is found. For T_{is} derived from OF($\nabla \times \vec{\tau}$) the Spearman Rank correlation to the NAO is much weaker than with constant OF and CF and not significant ($r_s = -0.06$).

For I_w, this lower correlation is caused by the way how OF is derived: The area of high positive correlation between the wind stress curl and OF is located close to that with a high negative correlation between the wind stress curl and I_w, as can be seen by a comparison of Figure 36 and 54. This is consistent with the picture that a high ice amount south of Storfjorden (high I_w) blocks the movment of ice out of the fjord and thereby lowering OF.

It also agrees with the finding of Schauer (1995) that an intense cyclonic wind field over the Barents Sea increases the BSW production. A lower OF leads to a smaller polynya area and reduced ice production, while a high I_w was found to be correlated positively to the polynya area and the ice production in Skogseth et al. (2004) when OF was kept constant. This indicates also that years with a high amount of ice in the Barents Sea do not necessary mean a high amount of ice and BSW production in Storfjorden. This agrees with Zang et al. (2000), who found that an increased number of leads in the Arctic Ocean caused by a diverging wind field can mean higher ice production even in the case of higher temperatures.

Therefore the correlation with the ice index and the output of the polynya model must be decreased when using OF($\nabla \times \vec{\tau}$) (which is correlated negatively to the I_w). The agreement between T_{is} with OF($\nabla \times \vec{\tau}$) and the

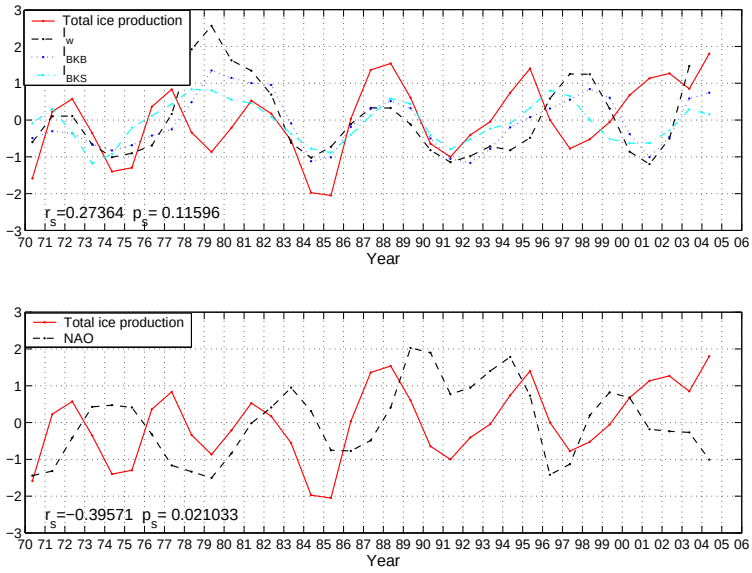

Figure 64: Upper panel: Two year running mean of T_{is} of a model run with OF($\nabla \times \vec{\tau}$) (solid line) compared to the ice indices: I_w (dashed line), I_{BKB} (dotted line) and I_{BKS} (dash dotted line). Lower panel: Two year running mean of T_{is} from a model run with OF($\nabla \times \vec{\tau}$) (solid line) and of the NAO (dashed line). All values are normalized. r_s and p_s are the Spearman Rank correlation coefficient and the significance level for T_{is} and I_w and the NAO, respectively.

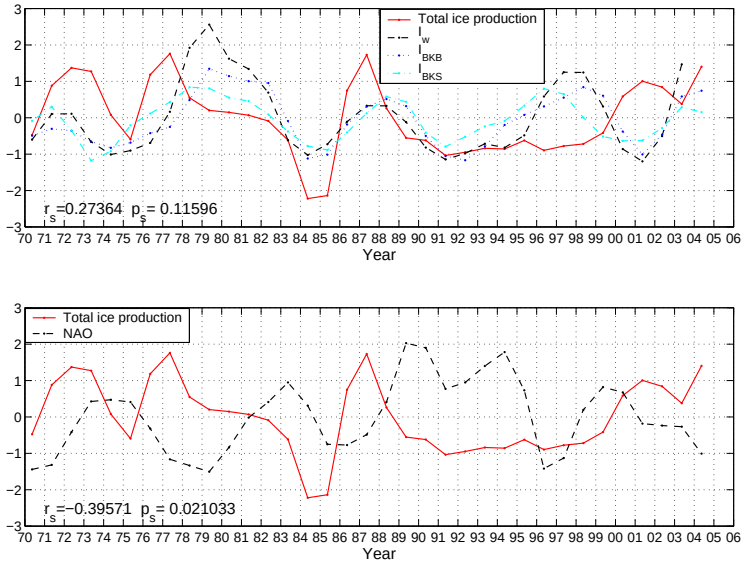

Figure 65: The same as Figure 64 but for OF(I_{BKS}).

measured salinites, however seemed to have improved for recent years compared to the case with constant OF, the polynya model results with varying factors may represent the conditions in Storfjorden better.

An interesting feature when comparing I_w and T_{is} is that they seem to agree rather well before 1992 but afterwards they are nearly anticorrelated (Figure 64). No proper explanation for this could be found. One possibility is, that the reproduction of OF was not successful before 1992, another reason may be that T_{is} shows an oscillation of about 5 years, while I_w rather oscillates with a period of 7 years. Because the periods are similar but not identical, the two time seriesncan oscillate in phase incidently for a short time.

To understand the decrease in correlation between T_{is} and the NAO one has to note that I_w and the NAO are not independent of each other. They are significantly negatively correlated, with $r_s = -0.44$ agreeing e.g. with Yi et al. (1999), who found an anticorrelation between the NAO and the ice concentration in the Greenland and Barents Sea. Thus a high NAO usually means a low I_w. There are two reasons for this connection: A high NAO was found to be connected to higher temperatures in the Barents Sea because of enhanced influx of warm water of Atlantic origin and a high NAO leads to a northeastward extension of the Atlantic storm track (Dickson et al. 2000). Both are connected to a smaller ice extent, the warmer temperatures through an enhanced melting or reduced freezing, while for the storm track, a higher number of low pressure system can break up the ice and lead to an enhanced melting (Holt and Martin 2001).

Therefore, a decrease in the magnitude of the correlation to the NAO may be just a result of the decreased correlation to the I_w explained above. This is also supported by the significant positive correlation found between the NAO and the reconstructed OF ($r_s = 0.59$). This indicates that a high NAO is connected to a high OF. This is probably due to the connection between the NAO and the ice extent in the western and central Barents Sea. A high NAO leads to less ice, therefore OF increases.

To improve the reproduction of OF and find an explanation for the variations of CF and so develope the polynya model for Storfjorden further more measurements are necessary. OF could be derived on a monthly basis from the wind stress curl or I_{BKS}, because the ice conditions can change significantly within one winter. For the wind stress curl it then becomes important that the ice extent is not only dependent on the current wind stress field but also on the ice extent and therefore wind stress field of the month before.

Additionally, it is possible that OF and CF depend on the time in the freezing season, because looser ice in the beginning and ice with more ridges at the end of the freezing season can be assumed to move much faster than the ice in the coldest part of the winter.

5 Conclusions

The wind stress fields and several ice indexes for the Barents Sea were investigated and an attemp was done to improve a polynya model for Storfjorden with the help of them. Eventough the quality of the wind stress data is questionable in the north before 1981 and the time series for the polynya model rather short, the followind conclusions could be drawn:

- On interannual time scales a close connection between the wind stress field and the sea ice extent in the Barents Sea could be found. In particular the northward wind stress component northeast of the considered area turned out to be important, but there are also links between the wind stress curl and divergence close to the ice edge to the ice extent.
- The NAO has a considerable influence on the ice extent in the Barents Sea, but especially in the eastern part local processes may be more important.
- Due to the connection between the wind stress curl and the ice extent it was possible to estimate the opening behaviour of the Storfjorden polynya using the wind stress curl in the area south of its entrance for recent years.
- Using the ice cover of an area south of Storfjorden instead of the wind stress curl confirmed the connection.
- The opening factor could be calculated for the past years. How reliable this is remains unclear, because there are too few measurements for comparison.

For following work it could be interesting to continue the on the polynya model for Storfjorden. Including tidal forces or defining opening and closing factors with a higher temporal resolution could further improve the model. More measurements are necessary to get a complete picture of the ice conditions and BSW production in Storfjorden.

6 Aknowledgements

I would like to thank especially Associate Prof. Frank Nilsen for his excellent scientific supervision and for giving me the possibility to work on Svabard, as close as possible to the field of my studies.

Further, I want to thank Prof. Mojib Latif and Prof. Tore Gammelsrød for helpfull remarks.

My special thanks to Dr. Rangheid Skogseth for providing and explaining the polynya model and her patience when helping me with the analysis of the satellite images.

I also want thank Børge Kvingedal calculating the ice index for the area near the fjord mouth of Storfjorden and providing further ice data.

Thanks also to Dr. Lars Asplin for providing the wind stress data, Dr. Ilker Fer for the salinity data and Inger Marie Nordin for the weather data from Hopen as well as Prof. Harald Loeng for allowing me to use his Barents Sea Ice Index.

Last but not least, I want to thank my parents for suporting me and my studies no matter how far away I decided to take them.

List of Figures

List of Tables

List of Abbreviations

AO	Arctic Oscillation
ASAR	Advanced syntitic aperature radar
AVHRR	Advanced very high resolution radar
BSW	Brine-enriched shelf water
CF	Closing factor for the polynya model
CTD	Conductivity-temperature-depth
DJF	December-February
DJFM	December-March
DJFMA	December-April
DMSP	Defence Meteorological Satillite Program
DNMI	Norwegian Meteorological Institute
ECMWF	European Center for Medium Range Weather Forecast
ERS	European remote sensing (satellite)
GIN	Greenland Iceland Norwegian Sea
HIRLAM	High Resolution Limited Area Model
I_{BKB}	Index of Barens Sea ice extent (by Børge Kvingedal)
I_{BKS}	Index of ice extent south of Storfjoden (by Børge Kvingedal)
I_w	Barens Sea winter ice index (by Harald Loeng)
IMR	Institute of Marine Research, Bergen
JJAS	June-September
NAO	North Atlantic Oscillation
NOAA	National Oceanographic and Atmospheric Administration
OF	Opening factor for the polynya model
SAR	Syntetic aperature radar
SSM/I	Special Sensor Microwave/Imager
WMO	World Meteorological Organisation

List of Symbols

A_0	Area of open water
A_{fp}	Area of fast and pack ice
A_t	Area of thin ice
B_1	Ice drift factor, $B_1 = 0.02$
C_d	Drag coefficient for neutral stability
d	Difference in statistical rank between corresponding variables
F_{net}	Net heat flux over open water
$F(\Phi_n - \Phi_0)$	Opening or closing Factor
H	Ice thickness
h_f	Equivalent thickness of frazil ice
H_{fp}	Ice growths thickness for fast and pack ice
H_t	Ice growths thickness for thin ice
L_s	Latent heat of fusion for sea ice, $L_s = 234.1 kJ kg^{-1}$
N	Length of time series
P_{fp}	Fraction of the area of fast and pack ice covered by leads
P_t	Fraction of the area of thin ice covered by leads
p	Confidence level
p_s	Spearman Rank confidence level
r	Correlation coefficient
r_s	Spearman Rank correlation coefficient
std	Standard deviation
$T_i s$	Total ice production in Storfjorden
Δt	Time step, $\Delta t = 6h$
U_n	10m wind speed at Hopen Island
var	Variance
V_f	Volume of frazil ice
V_i	Volume of ice from continuous grows
$W_{p,n}$	Polynya width at time n
$W_{p,n-1}$	Polynya width at time n-1
Θ	Culminative freezing degree days
ρ_a	Density of air
ρ_f	Frazil ice density, $\rho_f = 950 kg\, m^{-3}$
ρ_i	Density of ice from continuous grows, $\rho_i = 920 kg\, m^{-3}$
$\vec{\tau}$	Wind stress
τ_x	Eastward component of the wind stress
τ_y	Northward component of the wind stress
Φ_0	Wind direction ideal for ice transport out of Storfjorden, $\Phi_0 = 10^o$
Φ_n	10m wind direction at Hopen Island

References

[1] Ådlandsvik, B. and H. Loeng, 1991: "A study of the climatic system in the Barents Sea", pp. 45–49 in Sakshaug, E., C. C. E. Hopkins and N. A. Øritsland (eds.): "Proceedings of the Pro Mare Symposium on Polar Marine Ecology, Trondheim, 12–16 May 1990." *Polar Research*, vol. 10, no. 1

[2] Arbetter, T. E., A. H. Lynch and D. A. Bailey, 2004: "Relationship between synoptic forcing and polynya formation in the Cosmonaut Sea: 1. Polynya climatology", *Journal of Geophysical Research*, vol. 109, no. C04022

[3] Bailey, D. A., A. H. Lynch and T. E. Arbetter, 2004: "Relationship between synoptic forcing and polynya formation in the Cosmonaut Sea: 2. Regional climate model simulation", *Journal of Geophysical Research*, vol. 109, no. C04023

[4] Bengtsson, L., V. A. Semenov and O. M. Johannessen, 2004: "The Early Twenthieth- Century Warming in the Arctic – A Possible Mechanism", *Journal of Climate*, vol. 17, pp. 4045–4057

[5] Brümmer, B., G. Müller and H. Hoeber, 2003: "A Fram Strait cyclone: Properties and impact on ice drift as measured by aircraft and buoys", *Journal of Geophysical Research*, vol. 108, no. D7

[6] Cavalieri, D. J. and S. Martin, 1994: "The Contribution of Alaskan, Siberian and Canadian coastal polynyas to the cold halocline layer of the Arctic Ocean ", *Geophysiscal Research Letters*, vol. 99, no. C9, pp. 18343–18362

[7] Cressman, G. P., 1959: "An operational objective analysis system", *Monthly Weather Review*, vol. 87, no. 10, pp. 367–374

[8] Davidson, K. L., P. S. Guest and J. W. Glendening, 1992: "Determining realistic wind stress forcing fields for marine Arctic Regions", *Third Conference of Polar Meteorology and Oceanography, 29. September 1992*, pp. 44–47

[9] Deser, C., J. E. Walsh and M. S. Timlin, 2000: "Arctic Sea Ice Variability in the Context of Recent Atmospheric Circulation Trends", *Journal of Climate*, vol. 13, pp. 617–633

[10] Dickson, R. R., T. J. Osborn, J. W. Hurrell, J. Meincke, J. Bindheim, B. Adlandsvik, T. Vinje, G. Alekseev and W. Maslowski, 2000: "The

Arctic Ocean Response to the North Atlantic Oscillation", *Journal of Climate*, vol. 13, pp. 2671–2693

[11] ESA: "Envisat ASAR Quicklook pictures" *EOLI Catalogue* http://muis-env.esrin.esa.it:8080/servlets/template/welcome/entryPage2.vm

[12] Fang, Z., and J. M. Wallace, 1994: "Arctic sea ice variability on a time scale of weeks and its relation to atmospheric forcing", *Journal of Climate*, vol. 7, pp. 1897–1913

[13] Furnes, G. K., 1992: "Climate variations of oceanographic processes in the north European seas: a review of the 1970s and 1980s", *Continental Shelf Research*, vol. 12, no. 2/3, pp. 235–256

[14] Guest, P. S., J. W. Glendening and K. L. Davidson, 1995: "An observational and numerical study of wind stress variations within the marginal ice zones", *Journal of Geophysical Research*, vol. 100, no. C6, pp. 10887–10904

[15] Haarpaintner, J., J.-C. Gascard and P. M. Haugan, 2001: "Ice and brine formation in Storfjorden, Svalbard", *Journal of Geophysic Research*, vol. 106, no. C7, pp. 14001–14013

[16] Hilmer, M. and T. Jung, 2000: "Evidence for a recent change in the link between the North Atlantic Oscillation and Arctic sea ice export", *Geophysical Research Letters*, vol. 27, no. 7, pp. 989–992

[17] Holt, B. and S. Martin (2001), "The effectt of a storm on the 1992 summer ice cover of Beaufort, Chukchi, and East Sibirian Seas", *Journal of Geophysical Research*, vol. 106, no. C1, pp. 1017–1032

[18] Hurrel, J. W., 1995: "Decadal Trends in the North Atlantic Oscillation: Regional Temperatures and Precipitations", *Science*, vol. 289, pp. 676–679

[19] Ingvalsen, R., H. Loeng and L. Asplin, 2002: "Variability in the Atlantic inflow to the Barents Sea based on a one- year time series from moored current meters", *Continental Shelf Research*, vol. 22, pp. 505–519

[20] Ingvaldsen, R., L. Asplin and H. Loeng, 2004: "Velocity field of the western entrance to the Barents Sea", *Journal of Geophysic Reseach*, vol. 109, no. C03021

[21] Jones, P.D., T. Jónsson and D. Wheeler, 1997: "Extension to the North Atlantic Oscillation using early instrumental pressure observations from

Gibraltar and South-West Iceland", *Intrnational Journal of Climatology*, vol. 17, pp. 1433-1450.

[22] Kimura, N. and M. Wakatsuchi (2001), "Mechanisms for the variation of sea ice extent in the Northern Hemisphere", *Journal of Geophysical Research*, vol. 106, no. C12, pp. 31319–31331

[23] Kvingedal, B., 2005: "Sea- Ice Extent and Variability in the Nordic Seas, 1967–2002", submitted to *Journal of Climate*

[24] Kvingedal, B. and A. Sorteberg, 2005: "Atmospheric Forcing on the Barents Sea Ice", submitted to *Journal of Climate*

[25] Krahmann, G. and M. Visbeck, 2003: "Variability of the Northern Annular Mode's signature in winter sea ice concentrations", *Polar Research*, vol. 22, no. 1

[26] Leppäranta, M., 2005: "The Drift of Sea Ice", *Springer – Praxis Publishing Ltd. Chinchester, UK*

[27] Liu, J., J. A. Curry and Y. Hu, 2004: "Recent Arctic Sea Ice Variations: Connections to the Arctic Oscillation and the ENSO", *Geophysiscal Research Letters*, vol. 31, no. L09211

[28] Loeng, H., 1979: "A review of the sea ice conditions of the Barents Sea and the area west of Spitsbergen.(in Norwegian)", *Fisken og Havet*, vol. 2, pp. 29–75

[29] Loeng, H., 1991: "Features of the physical oceanographic conditions of the Barents Sea", Pp. 5–18 in Sakshaug, E., C. C. E. Hopkins and N. A. Øritsland (eds.): "Proceedings of the Pro Mare Symposium on Polar Marine Ecology, Trondheim, 12–16 May 1990." *Polar Research*, vol. 20, no. 1

[30] Makshtas, A. P., 2003: "Possible dynamic and thermal causes for the recent decrease in the sea ice in the Arctic Basin", *Journal of Geophysical Research*, vol. 108, no. C7

[31] Martin, S. and P. Kauffmann, 1981: "A field and labratory study of wave damping by grease ice", *Journal of Glaciology*, vol. 27, no. 96, pp. 283–313

[32] Martin, T. and T. Martin, 2004: "Variability of arctic Sea Ice Transports", submitted to *Journal of Geophysic Research*

[33] Maslanik, J. A., M. C. Serreze and R. G. Barry, 1996: "Recent decrease in Arctic summer ice cover and linkage to atmospheric circulation anomalies", *Geophysic Research Letters*, vol. 23, no. 13, pp. 1677–1680

[34] Maykut, G. A., 1986: "The surface heat and mass balance", in *The Geophysics of Sea Ice, NATO ASI Series*, vol. 146, pp. 395–463

[35] Murray, R. J. and I. Simmonds, 1995: "Response of climate and cyclones to reductions in Arctic sea ice", *Journal of Geophysical Research*, vol. 100, no. C3, pp. 4793–4806

[36] Müller, G.: www.wetterzentrale.de

[37] Nansen, F., 1902: "The oceanography of the North Polar Basin", *Norwegian North Polar Expedition 1893–1896, Scientific Results*, vol. 3, pp. 1–427

[38] NOAA: http://www.cpc.ncep.noaa.gov/products/precip/CWlink/ENSO/verf/new.ao.shtml

[39] Osborn, T.: http://www.cru.uea.ac.uk/∼timo/projpages/nao_update.htm

[40] Overland, J. E. and C. H. Pease, 1982: "Cyclone climatology of the Bering Sea and its relation to the sea ice extent", *Monthly Weather Review*, vol. 110, no. 1, pp. 5–13

[41] Press, W. H., S.A. Teukolsky, W.T. Vetterling and B.P. Flannery, 1992: "Numerical Recipies in FORTRAN – The Art of Scientific Computing" *Cambridge University Press*

[42] Press, W. H., S.A. Teukolsky, W.T. Vetterling and B.P. Flannery, 1996: "Numerical Recipies in Fortran 90 – The Art of Parallel Scientific Computing" *Cambridge University Press*

[43] Quadfasel, D., B. Rudels and K. Kurz: "Outflow of dense water from a Svalbard fjord into Fram Strait", *Deep-Sea Research Part A*, vol. 35, no. 7, pp. 1143–1150

[44] Reistad, M. and K. Iden, 1998: "Updating, correction and evaluation of a hindcast data base of air pressure wind and waves for the North Sea, the Norwegian Sea and the Barents Sea", *Research Report, Norwegian Meteorological Institute*, no. 9

[45] Richter-Menge, J. A., S. L. McNutt, J. E. Overland and R. Kwok, 2002: "Relating arctic pack ice stress and deformation under winter conditions", *Journal of Geophysical Research*, vol. 107, no. C10

[46] Rogers, J. C., L. Yang and L. Li, 2005: "The role of Fram Strait winter cyclones on sea ice flux and on Spitsbergen air temperatures", *Geophysical Research Letters*, vol. 32, no. L06709

[47] Sachs, L., 1992:"Angewandte Statistik", *Springer Verlag*, 7. edition, pp. 110-115

[48] Schauer, U., 1995: "The release of brine-enriched shelf water from Storfjord into the Norwegian Sea", *Journal of Geophysical Research*, vol. 100, no. C8, pp. 16015–16028

[49] Serreze, M. C., J. E. Box, R. G. Barry and J. E. Walsh, 1993: "Characteristics of arctic synoptic activity", *Meteorology and Atmospheric Physics*, vol. 51, no. 3–4, pp. 147–164

[50] Serreze, M. C., 1995: "Climatological aspects of cyclone developement and decay in the Arctic", *Atmospher-Ocean*, vol. 33, pp. 1–23

[51] Shapiro, I., R. Colony and T. Vinje, 2001: "April ice extent in the Barents Sea, 1850–2001", *Polar Research*, vol. 22, no. 1, pp. 5–10

[52] Skogseth, R., P. M. Haugan and J. Haarpaintner, 2004: "Ice and brine production in Storfjorden from four winters of satellite and in situ observations", *Journal of Geophysical Research*, vol. 109, no. C10008

[53] Skogseth, R., P.M. Haugan and M. Jakobsson, 2005: "Watermass transformation in Storfjorden", *Continental Shelf Research*, vol. 25, no. 5-6, pp. 667–695

[54] Smith, S. D., R. D. Muench and C. H. Pease, 1990: "Polynyas and Leads:An Overview of Physical Processes and Environment", *Journal of Geophysic Research*, vol. 95, no. C6, pp. 9461–9479

[55] Steele, M., J. H. Morison and T. B. Curtin, 1995: "Halocline water formation in the Barents Sea", *Journal of Geophysic Research*, vol. 100, no. C1, pp. 881–894

[56] Vinje, T. and Å. S. Kvambekk, 1991: "Barents Sea drift ice characteristics", Pp. 59–68 in Sakshaug, E., C. C. E. Hopkins and N. A. Øritsland (eds.): "Proceedings of the Pro Mare Symposium on Polar Marine Ecology", Trondheim, 12–16 May 1990. *Polar Research*, vol. 10, no. 1, pp. 59–68

[57] Vinje, T., 2001: "Anomalies and Trends of Sea-Ice Extent and Atmospheric Circulation in the Nordic Seas during the Period 1864–1998", *Journal of Climate*, vol. 14, pp. 255–267

[58] Walsh, J. E., W. L. Chapman and T. L. Shy, 1996: "Recent decrease of sea level pressure in the central Arctic", *Journal of Climate*, vol. 9, no. 2, pp. 480–486

[59] Walsh, J. E. and W. L. Chapman, 2001: "20th-century sea-ice variations from observational data", *Annals of Glaciology*, vol. 33, pp. 444–448

[60] Wang, J. and M. Ikeda, 2001: "Arctic sea-ice oscillations: regional and seasonal perspective", *Annals of Glaciology*, vol. 33, pp. 481–492

[61] Weisstein, E. W., 1999: "Spearman Rank Correlation Coefficient.", *MathWorld–A Wolfram Web Resource* http://mathworld.wolfram.com/SpearmanRankCorrelation Coefficient.html

[62] Winsor, P. and G. Björk, 2000: "Polynya activity in the Arctic Ocean from 1958 to 1997", *Journal of Geophysical Research*, vol. 105, no. C4, pp. 8789–8803

[63] WMO, 1972: "WMO Sea-ice Nomenclature", *WMO*, no. 259, TP. 145

[64] Wu, B., J. Wang and J. Walsh, 2004: "Possible Feedback of Winter Sea Ice in the Greenland and Barents Sea on the Local Atmosphere", *Monthly Weather Review*, vol. 132, pp. 1868–1876

[65] Yi, D., L. A. Mysak and S. A. Venegas, 1999: "Decadal-to-interdecadal Fluctuations of Arctic Sea-Ice Cover and the Atmospheric Circulation during 1954–1994", *Atmosphere-Ocean*, vol. 37, no. 4, pp. 389–415

[66] Zang, J. L., D. Rothrock and M. Steele: " Recent changes in Arctic sea ice: The interplay between ice dynamics and thermodynamics", *Journal of Climate*, vol. 13, no. 17, pp. 3099–3114

Erklärung

Hiermit bestätige ich, dass ich die vorliegende Diplomarbeit selbständig verfasst und keine anderen als die angegebenen Quellen als Hilfsmittel verwendet habe.

Ich versichere, dass diese Arbeit noch nicht zur Erlangung eines Diplomgrades an anderer Stelle vorgelegen hat.

Kiel, 6. Juni 2005

Katja Weigel